Quantifying US Landfill Methane Emissions Using TROPOMI+GOSAT Satellite Data

A Thesis Presented

by

Gabriel Maxemin

to

The Department of Earth and Planetary Sciences

in partial fulfillment of the requirements

for a degree with honors

of Bachelor of Arts

April 2024

Harvard College

Abstract

Methane is a greenhouse gas with a short atmospheric lifetime and strong warming potential. Reduction of anthropogenic methane emissions is thus a significant way to combat climate change. Recent literature has suggested discrepancies between "top-down" and "bottom-up" estimates of landfill emissions. In this study, we explore this discrepancy through a top-down estimate that employs a blended TROPOMI+GOSAT satellite data set and focuses on landfills sources over the United States during recent years, up to 2022. Through wind rotation of methane satellite observations, oversampling, and an integrated mass enhancement method, we quantify methane emission rates. We employ these methods on eight landfills and explore associations between methane emission rates and landfill characteristics. In most cases, we see greater methane emission rates for our top-down estimates compared to the bottom-up inventory report estimates. Assuming no regional differences in landfill methane emissions reporting across the United States, we suggest that bottom-up methane emission reports are under-reported as is evidenced by the discrepancy with our top-down estimates employing TROPOMI+GOSAT data. For 2022 and compared to our top-down estimates, methane emission rates for the eight selected landfills range in how much they underestimate emissions from 1.34 $\mathrm{Gg\,a^{-1}}$ to 13.49 $\mathrm{Gg\,a^{-1}}$. Two landfill characteristics, cover type and waste-containing surface area, show strong correlations with the discrepancy in emission estimates. The top-down methane emission rate estimates, as well as the observed difference in methane emission rates, can inform the parameterization of bottom-up functions employed for emissions reporting.

Contents

List of Figures

List of Tables

Acknowledgements

The research project was conducted within the Department of Earth and Planetary Sciences at Harvard University. I worked in the Atmospheric Chemistry Modeling Group (ACMG) with advising from Daniel Jacob and Nicholas Balasus.

I learned a lot through this experience and I'm thankful to both of my advisors for providing so much support. I'm grateful to Daniel for the opportunity to join his group and for his continued willingness to chat with me about thesis and non-thesis work. I want to also thank Nick for his patience as I debugged my code and asked dozens of questions, for showing me neater and more optimized coding techniques, and for working with me through times of chaos. I'm thankful to the ACMG group for making me feel part of the team from the very first time I joined the lab. I also want to acknowledge Hannah Nesser who talked to me about her own work on landfills and provided some interesting avenues to explore for the project.

This endeavor would have been a lot more difficult without my friends, mentors, and community at Harvard. I express my gratitude to everyone who supported me and provided words of encouragement.

I received financial support from the Department of Earth and Planetary Sciences for this project. Additionally, funding from the ACMG allowed me to work on the project during the summer.

The blended TROPOMI+GOSAT data set I used is available at https://dataverse.harvard.edu/dataverse/blended-tropomi-gosat-methane (*Balasus*

et al., 2023). I used the EPA GHGRP FLIGHT tool available at https://ghgdata.epa.gov/ghgp/main.do (*US EPA*, 2022) as well as GHGRP data sets available at https://www.epa.gov/ghgreporting/data-sets (*US EPA*, 2014).

Chapter 1

Introduction

1.1 Methane

Methane CH_4 is a greenhouse gas with a strong global warming potential (GWP) and a short atmospheric lifetime, making it a significant contributor to climate change. Its atmospheric lifetime is estimated at 9.1 ± 0.9 y (*Prather et al.*, 2012). This makes methane emission reduction attractive for rapid near-future impacts. GWP is measured with CO_2 as the reference where the GWP of CO_2 is 1. CH_4 has a GWP of 28 over a time period of 100 years (*Myhre et al.*, 2013). Anthropogenic sources make up around 60% of global methane emissions (*Saunois et al.*, 2020). Reduction of anthropogenic methane emissions is therefore significant in climate change mitigation.

1.2 Satellite Data

Methane emissions are calculated in two main ways. A "top-down" approach involves observations of atmospheric methane which are used to estimate methane emissions. In contrast, a "bottom-up" approach employs activity data for emission inventories.

Satellites observe atmospheric methane columns via measurements of backscattered solar shortwave infrared radiation (SWIR; *Jacob et al.* (2016)). Two high-precision instruments with regional to global coverage, classified as area

flux mappers (*Jacob et al.*, 2016), are the TANSO-FTS instrument aboard the Greenhouse Gases Observing Satellite (GOSAT) satellite and the TROPOspheric Monitoring Instrument (TROPOMI) aboard the Sentinel-5 Precursor satellite. TANSO-FTS has collected global methane observations since 2009 with 10.5 km circular pixel footprints spaced apart by ∼263 km across-track and ∼283 km along-track (*Parker et al.*, 2020). TROPOMI has daily global observations and in August 2019 began capturing at a 5.5 x 7 km^2 resolution (*Lorente et al.*, 2021). GOSAT measures methane in the 1.65 µm wavelength band through a CO_2 proxy, being then prone to errors in the prior estimate of CO_2 (*Parker et al.*, 2011). In contrast, TROPOMI measures in the 2.3 µm without a CO_2 proxy and using a physics based approach, which has greater errors induced by scattering than the CO_2 proxy method (*Butz et al.*, 2012). TROPOMI observations are subject to different biases. One of these is the misrepresentation of surface albedo (*Jongaramrungruang et al.*, 2021). Another bias comes from aerosols and cirrus clouds scattering the radiation (*Aben et al.*, 2007; *Butz et al.*, 2010; *Schepers et al.*, 2012).

Here, we use a blended TROPOMI+GOSAT product from *Balasus et al.* (2023). The blended data set provides a favorable compromise between the higher data density of TROPOMI and the greater data quality of GOSAT.

1.3 Bottom-up Data

Bottom-up estimates are calculated based on activity levels and emission factors (*IPCC*, 2019). For example, this could take the form of multiplying the amount of waste in landfill (activity level) by methane emitted per unit area of the landfill (emission factor). Imprecise and unknown emission factors then increase uncertainty in bottom-up estimates.

1.3.1 EPA GHGRP

The United States Environmental Protection Agency (EPA) reports annual methane inventories for its Greenhouse Gas Reporting Program (GHGRP). Among those required to report are facilities emitting more than 25,000 metric tons of greenhouse gases per year. More specifically for landfills, those emitting more than 1,190 metric tons of CH_4 per year are required to report (*US EPA*, 2014). Methane emissions are calculated as a function of quantity of each type of waste in a landfill. Emissions are also functions of correction factors, rate constants, and fractions, of which most have default values provided by the EPA or can be altered based on site-specific information.

1.4 Landfills

According to the EPA, landfills accounted for 17% of total methane emissions in the United States in 2022. Following enteric fermentation and natural gas systems, landfills were the third largest anthropogenic source of methane emissions in 2022 (*US EPA*, 2024). There exist discrepancies between top-down and bottom estimates. Landfill methane emission estimates for 2019 derived from satellites are 51% greater than those reported by the US Environmental Protection Agency Greenhouse Gas Emissions Inventory (*Nesser et al.*, 2023).

Landfill gas contains, among hundreds of other gases, 40-60% methane and can be produced through bacterial decomposition, phase changes via volatilization, and chemical reactions within the waste. Different landfill conditions like moisture content, oxygen concentration, and temperature may impact landfill gas production (*ATSDR*, 2001).

In 2022, the EPA reports a total of 1123 municipal landfills, accounting for 83 million metric tons CO_2e of greenhouse gas emissions (*US EPA*, 2022).

Municipal landfills are those receiving household waste and other types of nonhazardous waste (*US EPA*, 2016a). Municipal landfills, because of their organic waste, are prominent sources of methane emissions generated anthropogenically (*US EPA*, 2016b).

Chapter 2

Data and Methods

2.1 Wind Rotation

For a given landfill, we are interested in estimating its methane emissions. TROPOMI+GOSAT satellite data provide methane concentration observations for a given pixel area. The satellite observation does not directly inform us on the methane emission rate. In order to understand the methane emission source that would give rise to the methane concentration that the satellites observe, we employ a wind rotation technique.

In *Zuo et al.* (2023), the authors employ wind direction and speed data for each satellite pixel to analyze the downwind structure of HCHO. We adopt a wind rotation technique that allows the remapping of satellite observations according to a source wind (*de Foy et al.*, 2015; *Fioletov et al.*, 2016; *Lu et al.*, 2015; *Pommier et al.*, 2013; *Valin et al.*, 2013; *Beirle et al.*, 2011). We choose a center $(x_0, y_0) = (0, 0)$, calculate the distance μ of the pixel to x_0, and rotate the pixel an angle θ to align the pixel along the wind direction. We rotate a satellite point centered at (x, y) to (x_{new}, y_{new}):

$$\begin{aligned} x_{new} &= x\cos(-\theta) + y\sin(-\theta) \\ y_{new} &= -x\sin(-\theta) + y\cos(-\theta) \end{aligned} \tag{2.1}$$

Figure 2.1 shows an example of the wind rotation method.

We use wind data sourced from the National Oceanic and Atmospheric

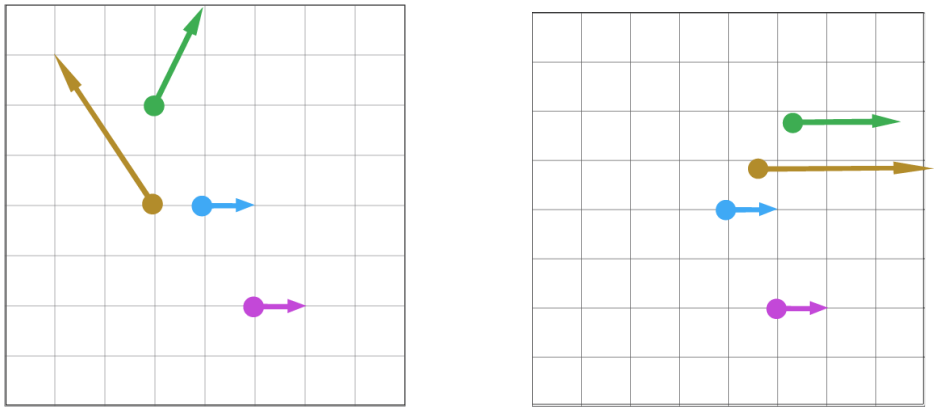

(a) (b)

Figure 2.1: (a) Wind vectors before rotation. (b) Wind vectors after rotation. The blue circle represents the source, and the blue vector represents the downwind direction.

Administration High-Resolution Rapid Refresh (HRRR) (*Dowell et al.*, 2022). The data has a spatial resolution of 3 km and temporal resolution of 1 h.

We begin with a municipal landfill identified from the GHGRP. We choose a set of coordinates within the landfill space as the source center (x_0, y_0). All satellite observations surrounding the source center are rotated following the source's wind direction.

To be more certain that the observed methane concentrations are due to the landfill and not to an external source, we inspect the infrastructure of the vicinity and identify other possible source candidates such as oil and gas plants and farms. We rotate around these locations and through visual inspection of the plumes we ensure that the plume arises from the landfill independently.

2.2 Oversampling

After wind rotation, we oversample the data to achieve fine-resolution mapping of the methane emissions.

One technique to visualize a single snapshot of the satellite data is to

project the data onto a 2-dimensional latitude versus longitude map and average the data into spatial grid cells. This technique limits the possible resolution of these visualizations based on the observational density at each grid cell for the given time snapshot. In order to access finer resolution, we employ a "tessellation" approach to oversample our data as described in *Sun et al.* (2018). For a given period of time, all observations captured within a pre-defined grid cell are weighed and averaged onto that grid cell. In this way, we achieve a finer spatial resolution since we have more observations at each grid cell, consequently sacrificing the time dimension.

The tessellation method weighs the overlapping area between an irregularly-shaped polygon satellite observation and a rectangular grid cell. The oversampling equations provide a way to calculate a weighted average of the observations for each grid cell. From *Sun et al.* (2018), upon oversampling, a grid cell will have a methane concentration $C(j)$ [ppb]:

$$C(j) = \frac{A(j)}{B(j)} \tag{2.2}$$

where

$$A(j) = \sum_i \frac{\Omega(i) S(i,j)}{\sum_j S(i,j)} \tag{2.3}$$

$$B(j) = \sum_i \frac{S(i,j)}{\sum_j S(i,j)} \tag{2.4}$$

In these equations, we refer to pixel i and grid cell j. $\Omega(i)$ [ppb] represents a pixel's methane column, $S(i,j)$ [m^2] is the overlapping area between a pixel i and grid cell j, and $\sum_j S(i,j)$ [m^2] represents the total area of a pixel. *Sun et al.* (2018) include an uncertainty term which we have removed since its impact on the weighted average concentrations was minimal. The $\sum_j S(i,j)$ term assumes that pixel boundaries all fit inside the grid within which we

oversample.

In Figure 2.2, we demonstrate a visualization of satellite observation pixels oversampled onto a grid.

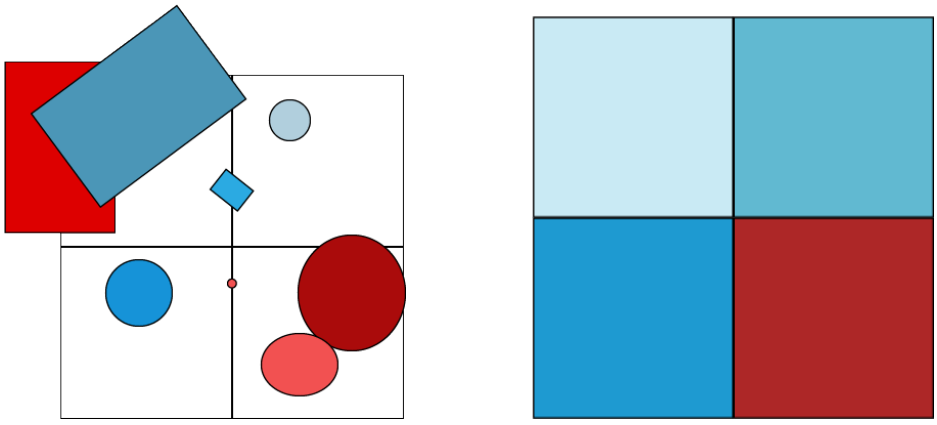

(a) (b)

Figure 2.2: (a) Satellite observation pixels with different geometries. The colors represent arbitrary values of a measurement (e.g. different methane concentrations). (b) Oversampled grid. The satellite pixels from (a) were weighted and averaged onto a defined grid

Similarly, we oversample the dry air column densities with the same weights as the methane concentrations. We use $\Omega_{air}(i)$ [kg m^{-2}], a pixel's dry air column, to give us the oversampled dry air column of a grid cell $\sigma_{air}(j)$:

$$\sigma_{air}(j) = \frac{A_{air}(j)}{B(j)} \tag{2.5}$$

where

$$A_{air}(j) = \sum_i \frac{\Omega_{air}(i)S(i,j)}{\sum_j S(i,j)} \tag{2.6}$$

We have filtered out any pixels over water and those most prone to coastal biases, described in Appendix D of *Balasus et al.* (2023).

For a given resolution for oversampling, we require a minimum number of observations to make inferences about a grid cell. For a native resolution of a x b, oversampling at c x d means that we should have $\frac{a}{c} \times \frac{b}{d}$ observations

per grid cell oversampled to preserve the information content of the original data. The original TROPOMI+GOSAT data has resolution 5.5 x 7 km^2. If we oversample with 0.01°x 0.01°grid cells, roughly translating to 1 x 1 km^2, we require approximately 40 observations per grid cell as a minimum.

2.3 Integrated Mass Enhancement

To obtain an estimate of the emission rate from a landfill, we employ an integrated mass enhancement (IME) method. This method, adapted from *Frankenberg et al.* (2016), estimates the mass of methane from a plume in the context of its background. The IME [kg] is a function of an enhancement $C(j) - C_b$ [ppb] where $C(j)$ is the methane concentration of the oversampled grid cell and C_b is the background methane concentration. The methane plume is characterized as being the region with methane concentrations above a specified percentile for a given region. The percentile is a parameter that we tune for each landfill individually. We vary the plume percentile to estimate the uncertainty of our methodology, explained in the next section. C_b is calculated as the average methane concentration from the layers of cells immediately surrounding the plume. The number of cells is another parameter that we tune for each landfill individually. The IME is also a function of the oversampled dry air column σ_{air} [10^{-9} mol m^{-2}], the area of the grid cell A_j [m^2], and the molar mass of methane M_{CH_4} [kg mol^{-1}]. We take the sum over all grid cells within the plume to obtain:

$$IME = \sum_j (C(j) - C_b) * \sigma_{air} * A_j * M_{CH_4} \tag{2.7}$$

The landfill source methane emission rate Q [kg s^{-1}] and IME [kg] hold a

linear relationship (*Frankenberg et al.*, 2016; *Varon et al.*, 2018):

$$Q = \frac{U}{L} \cdot IME \tag{2.8}$$

where we take the length scale L [m] to be the square root of the area of the plume mask and the effective wind speed U [m s^{-1}] to be the average wind speed at the landfill source location.

2.4 Parameters and Uncertainty

For each landfill, we vary two parameters when performing the oversampling. One parameter is plume percentile, which defines the region that constitutes a plume. For example, with a plume percentile of 98.5, the plume area within a given region is defined as the area with methane concentrations above the 98.5th percentile as compared to the rest of the region. Each landfill has different percentiles that give rise to what one can visually characterize as a plume pointing downwind. For example, one landfill may have an oversampled map that shows a downwind plume at a 99 plume percentile but not at a 96 plume percentile.

Our other parameter is background cells. This is the number of cells making up the width of the region immediately surrounding the perimeter of the plume. We use this belt of cells to calculate the background methane concentration. In other words, these cells represent what the methane concentration of the region would be in the absence of the landfill. For each landfill, we typically vary this parameter from one to three background cells. Figure 2.3 shows an example with the parameter set to one background cell.

For a given landfill, we take the methane emission rate Q to be the average

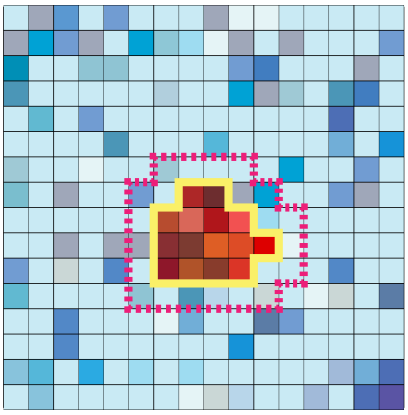

Figure 2.3: Integrated mass enhancement (IME). The grid is oversampled with blue indicating lower methane concentrations and red indicating higher methane concentrations. A yellow line traces the perimeter of a methane plume. The region between the yellow line and dashed pink line has a width of one cell, and it is the region used to calculate the background methane concentration.

of all methane emission rate estimates Q_n for that landfill:

$$Q = \frac{1}{N} \cdot \sum_n Q_n \tag{2.9}$$

where N is the number of estimates. For example, if we vary each of our parameters by having a 98.5, 99, and 99.5 plume percentile as well as one, two, and three background cells, we get a total of nine combinations. This results in nine methane emission rate estimates, so we would take the landfill's methane emission rate to be the average of the nine.

We calculate the uncertainty ΔQ by taking into account the range in emission rate estimates:

$$\Delta Q = \frac{1}{2} \cdot (Q_{max} - Q_{min}) \tag{2.10}$$

where Q_{max} and Q_{min} are the highest and lowest of the Q_n estimates.

2.5 Landfill Characteristic Analysis

We use data provided by the EPA GHGRP Facility Level Information on GreenHouse gases Tool (FLIGHT) tool (*US EPA*, 2022) to acquire information about our selected landfills' characteristics. We measure the linear correlation between our top-down estimates and landfill characteristics like cover type, waste-containing surface area, and the methane emission rate reported by the GHGRP with Pearson correlation coefficients. This allows for an analysis of the landfill's methane emission rate in the context of its own characteristics as well as in comparison to other landfills.

Chapter 3

Results

3.1 Oversampled Data Overview

We collected data for eight landfills across the continental United States. Figure 3.1 shows a map of the continental United States methane concentrations with landfills overlaid using data from 2022. The northwestern portion of the US suffers from low data density, and so do some regions across the northeast. This data density pattern is also evident when expanding to a larger time period of 2019 to 2022, as seen in Figure 3.3. Figure 3.2 and Figure 3.4 show the continental United States oversampled maps with landfills overlaid. We focus on regions with greater data density for our analysis of landfills. The data density for 2022 and for 2019 to 2022 is more clearly displayed in Figures 3.5 and 3.6, noting the difference in the color scales.

3.2 Landfill Example: Laurel Ridge Landfill

We identified landfills spatially isolated from other landfills. As an example, here we follow the oversampling process for Laurel Ridge Landfill located in Lily, Kentucky. Figure 3.7 shows 2022 oversampled data maps for Kentucky and the surrounding area.

From here, we identified Laurel Ridge Landfill as an isolated landfill. Figure 3.8 exemplifies this, showing Laurel Ridge landfill as the only GHGRP-

identified facility in the vicinity.

The wind rotation and oversampling procedure produced Figure 3.9. We can see a plume-like structure pointing downwind. Because of this structure and the landfill's spatial isolation, we can be more certain that the integrated mass enhancement (IME) method will be appropriate. In Figure 3.9, we have chosen two parameters: a plume percentile of 98.5 and a background cell number of two. However, this represents just one combination of parameters used.

For Laurel Ridge Landfill, we varied the definition of the plume to be the area with methane concentrations in the 98.5, 99, and 99.25 percentiles. Additionally, we can vary the definition of the background methane concentration: one, two, or three grid cells extending beyond the perimeter of the plume. Varying these two parameters yields different methane emission rates for the landfill. Using a percentile of 98.5 and a background cell number of 2, we get the following results from the IME method using 2022 data:

$$L = 10\,515.95\,\mathrm{m},\ U = 5.21\,\mathrm{m\,s^{-1}},\ IME = 976.72\,\mathrm{kg}$$

$$Q = \frac{U}{L} \cdot IME = 15.26\,\mathrm{Gg\,a^{-1}}$$

Varying the percentile and background cell parameters, we get the results displayed in Table 3.1. Figure 3.10 shows each plume variation for 2022. Figure 3.17, Figure 3.18, and Figure 3.19 show the plume variations for 2019, 2020, and 2021, respectively.

Consolidating the methane emission rate as the average of these emission rates and the uncertainty as half of the range, we obtain:

$$Q_{TROPOMI+GOSAT,2022} = (11.56 \pm 6.25)\,\mathrm{Gg\,a^{-1}}$$

The GHGRP reports the annual methane emissions found in Table 3.2 for Laurel Ridge Landfill.

Percentile	Background Cell Number	$Q(\mathrm{Gg\,a^{-1}})$
98.5	1	11.83
98.5	2	15.26
98.5	3	18.45
99	1	8.04
99	2	10.95
99	3	13.84
99.25	1	5.96
99.25	2	8.56
99.25	3	11.16

Table 3.1: Methane emission rate top-down estimates for Laurel Ridge Landfill in 2022. We vary two parameters: plume percentile and background cell number to obtain different estimates.

Year	$M_{\mathrm{CH_4}}$ (Gg)
2019	10.10
2020	2.50
2021	1.80
2022	1.70

Table 3.2: GHGRP methane emission estimates for Laurel Ridge Landfill.

From the GHGRP data, we obtain landfill emission rates of

$$Q_{GHGRP,2022} = 1.7\,\mathrm{Gg\,a^{-1}}$$

$$Q_{GHGRP,2019to2022} = 4.0\,\mathrm{Gg\,a^{-1}}$$

$Q_{GHGRP,2019to2022}$ represents the average Q_{GHGRP} for 2019 to 2022. Table 3.3 shows the yearly methane emission rate calculated using oversampled TROPOMI+GOSAT data Q in comparison to the EPA GHGRP emission rate Q_{GHGRP}.

We get $Q_{GHGRP,2019to2022}$ as the average Q_{GHGRP} for 2019 to 2022, and its uncertainty as the average uncertainty for 2019 to 2022. Comparing emission rates, we get:

$$Q_{GHGRP,2019to2022} = 4.0\,\mathrm{Gg\,a^{-1}}$$

Year	Q ($\mathrm{Gg\,a^{-1}}$)	Q_{GHGRP} ($\mathrm{Gg\,a^{-1}}$)
2019	13.21±6.65	10.10
2020	6.28±3.01	2.50
2021	13.28±7.27	1.80
2022	11.56±6.25	1.70

Table 3.3: Top-down versus bottom-up methane emission rates for Laurel Ridge Landfill.

$$Q_{GHGRP,2022} = 1.7\,\mathrm{Gg\,a^{-1}}$$

$$Q_{TROPOMI+GOSAT,2019to2022} = (11.08 \pm 5.80)\,\mathrm{Gg\,a^{-1}}$$

$$Q_{TROPOMI+GOSAT,2022} = (11.56 \pm 6.25)\,\mathrm{Gg\,a^{-1}}$$

This comparison is visualized in Figure 3.11.

3.3 All Landfills

Table 3.4, Table 3.5, Table 3.6, and Table 3.7 summarize the comparison between the GHGRP CH_4 emission estimates and our estimates employing oversampled TROPOMI+GOSAT data for 2019, 2020, 2021, and 2022, respectively. Figure 3.14 provides a visualization of these comparisons.

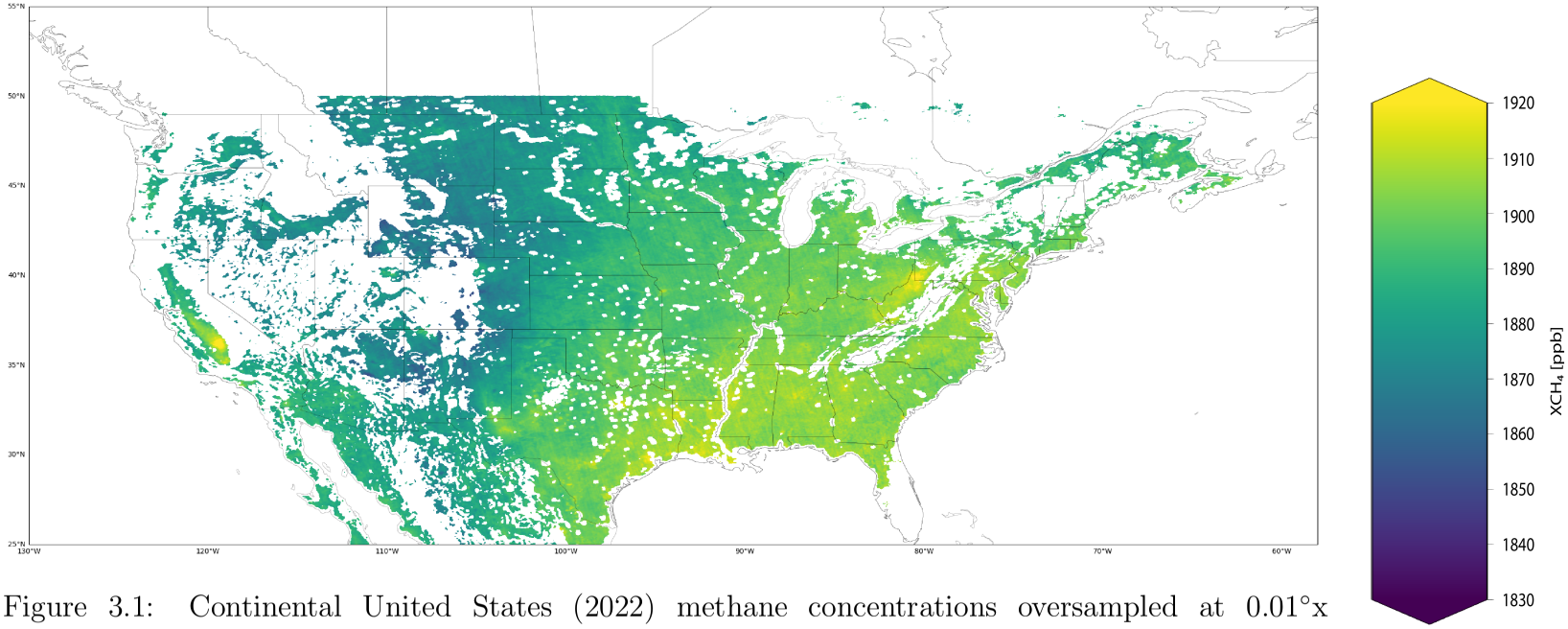

Figure 3.1: Continental United States (2022) methane concentrations oversampled at 0.01°x 00.1°resolution. Only grid cells with more than 40 observations are displayed; other regions are in white.

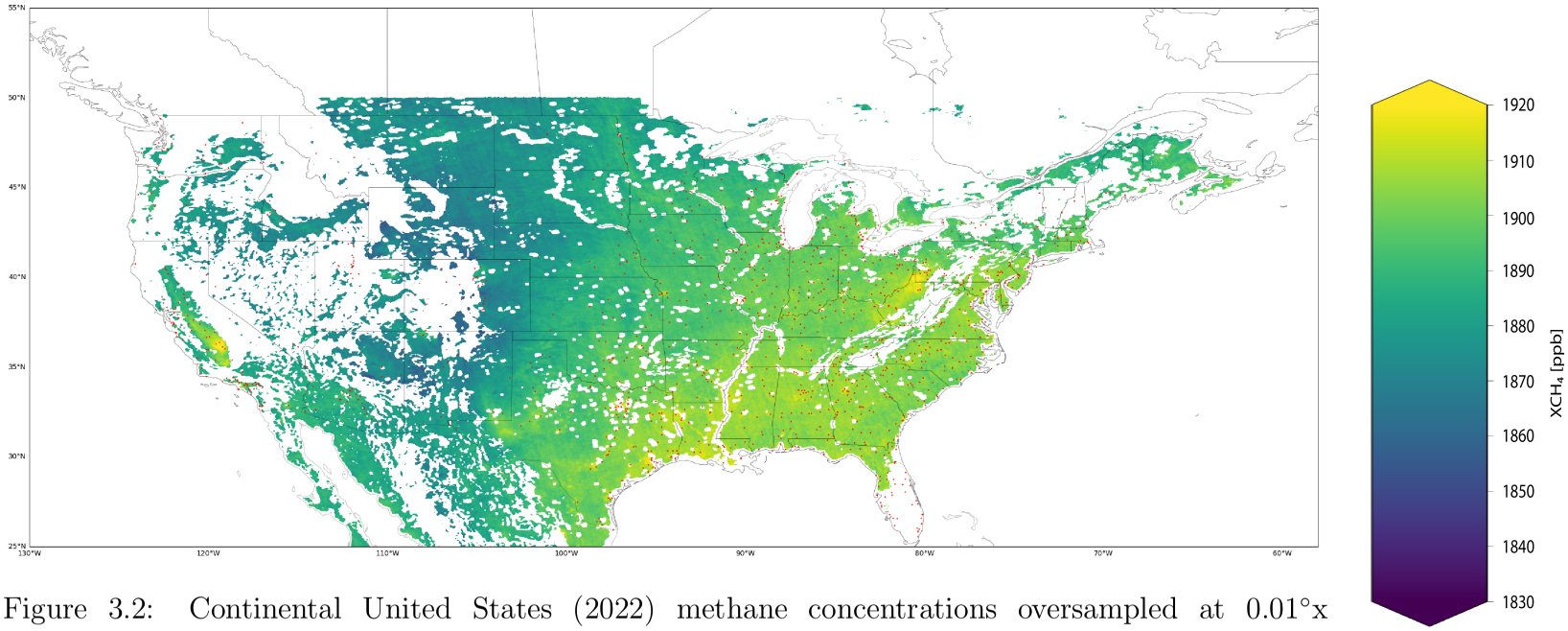

Figure 3.2: Continental United States (2022) methane concentrations oversampled at 0.01°x 00.1°resolution with landfills overlaid in red. Only grid cells with more than 40 observations are displayed; other regions are in white. Red dots indicate landfills as reported from the GHGRP.

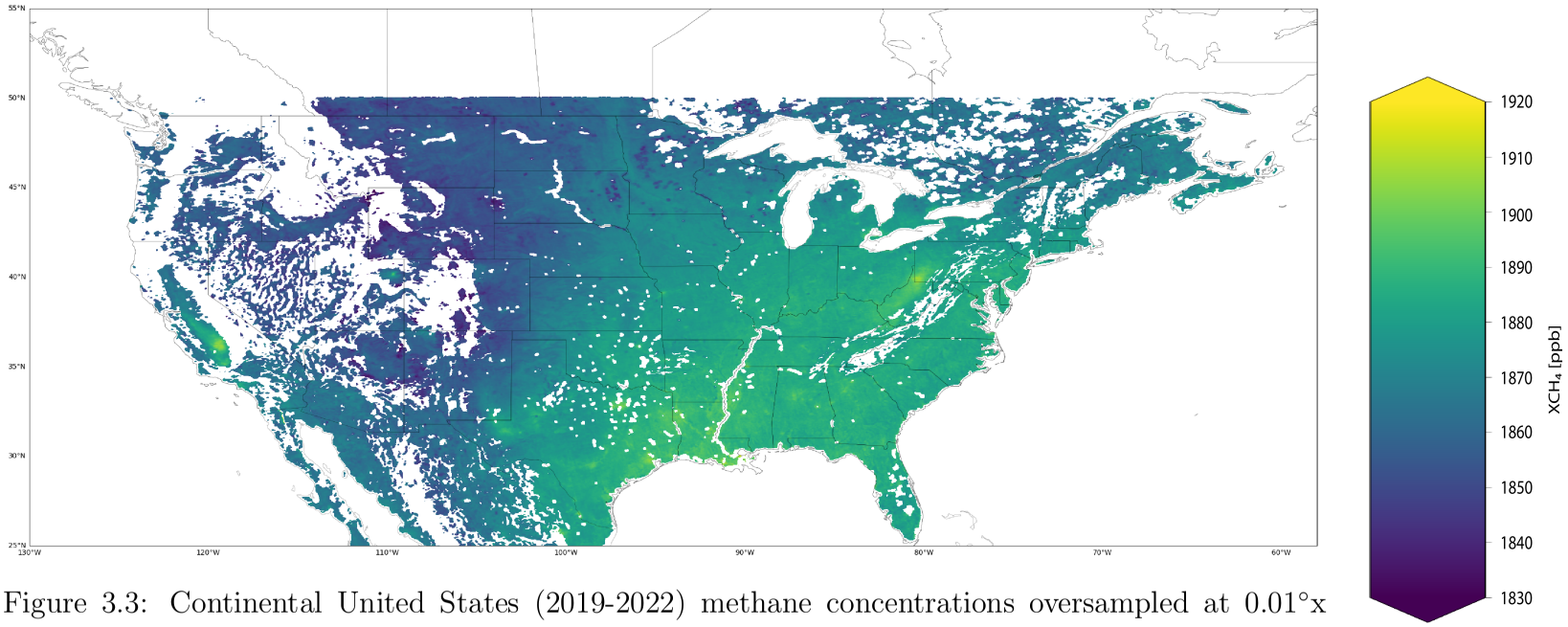

Figure 3.3: Continental United States (2019-2022) methane concentrations oversampled at 0.01°x 00.1°resolution. Only grid cells with more than 40 observations are displayed; other regions are in white.

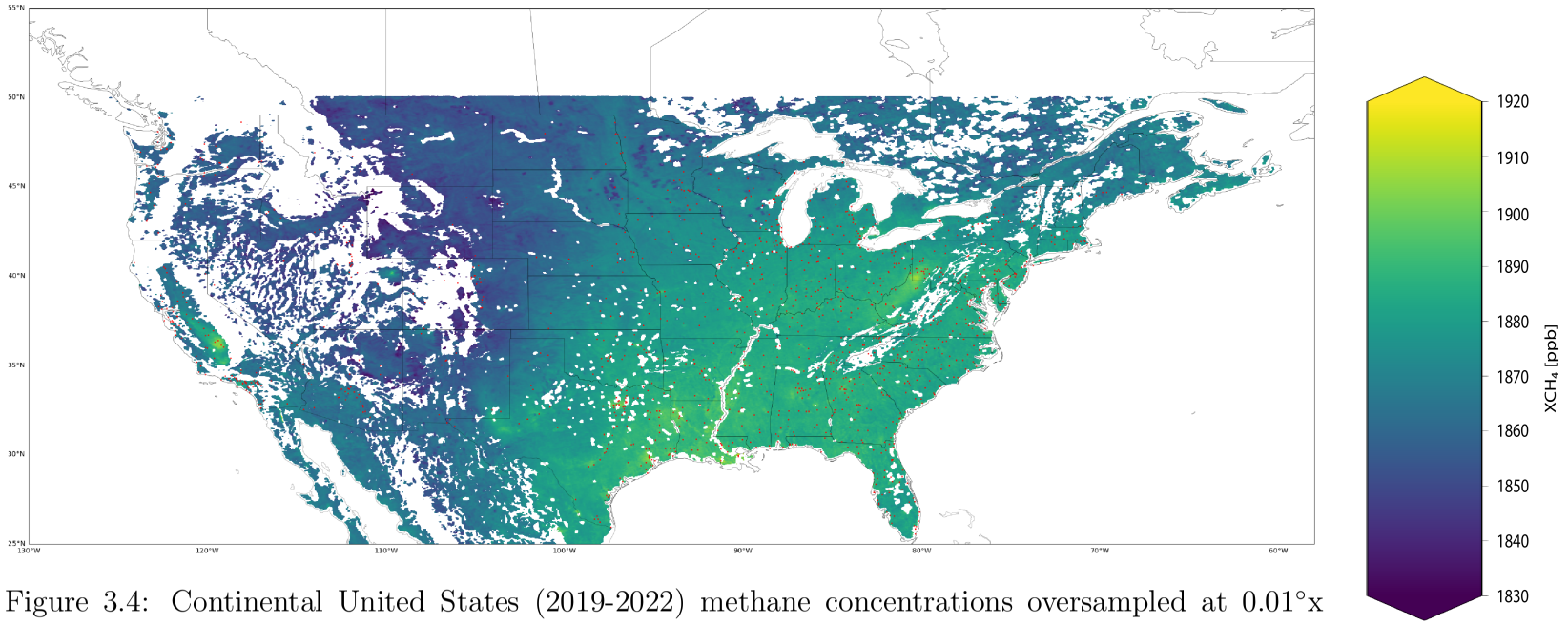

Figure 3.4: Continental United States (2019-2022) methane concentrations oversampled at 0.01°x 00.1°resolution. Only grid cells with more than 40 observations are displayed; other regions are in white.

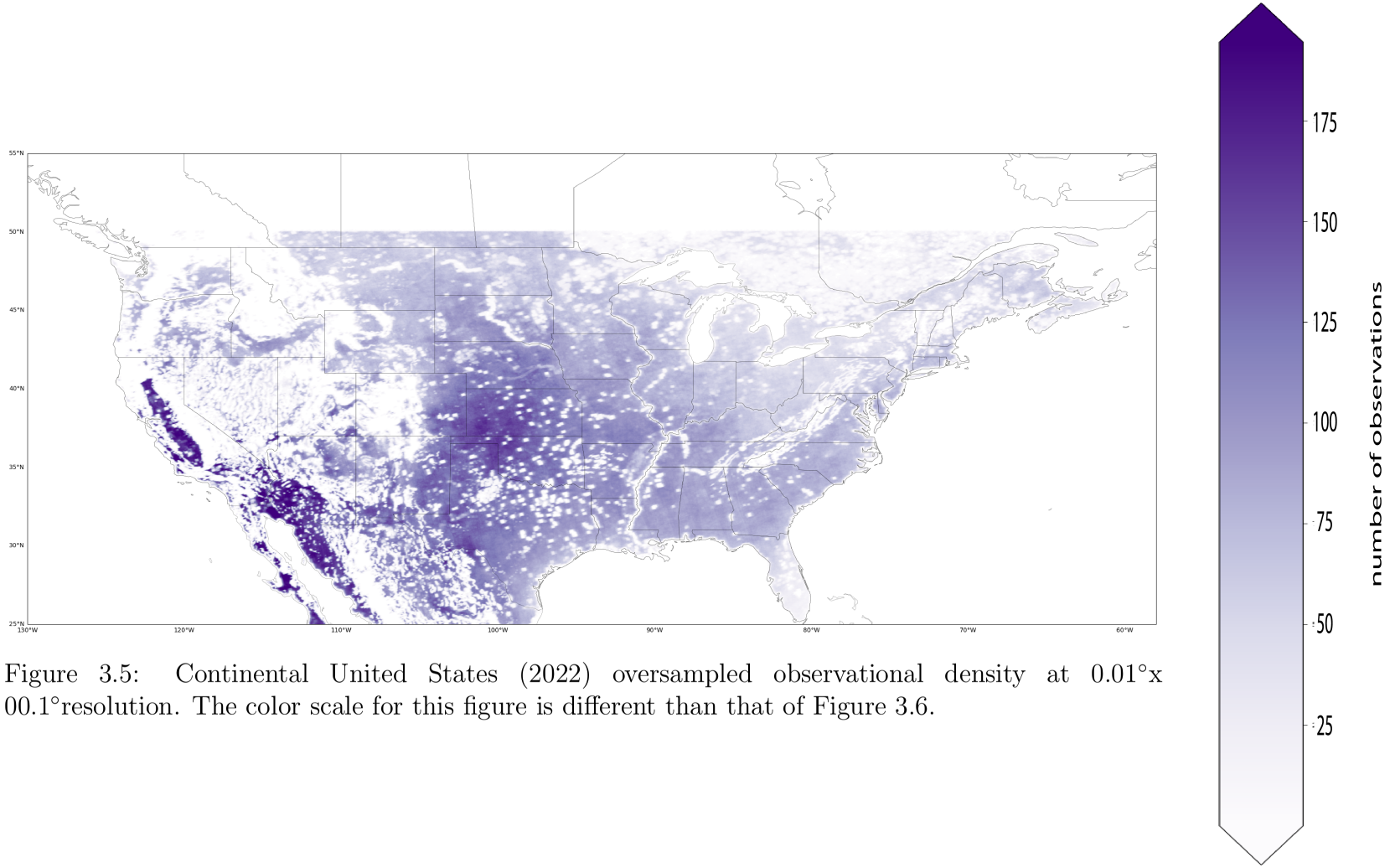

Figure 3.5: Continental United States (2022) oversampled observational density at 0.01°x 00.1°resolution. The color scale for this figure is different than that of Figure 3.6.

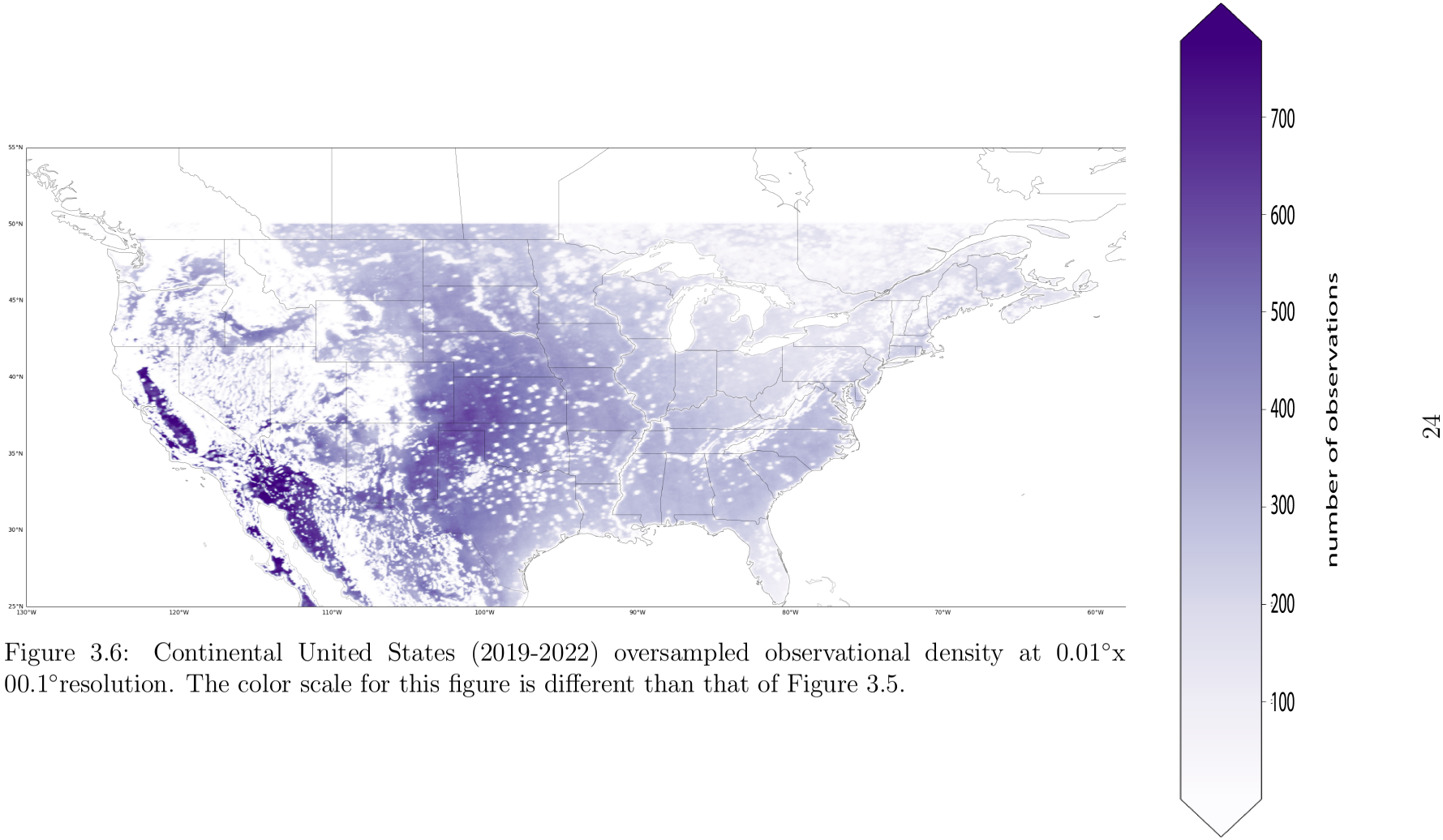

Figure 3.6: Continental United States (2019-2022) oversampled observational density at 0.01°x 00.1°resolution. The color scale for this figure is different than that of Figure 3.5.

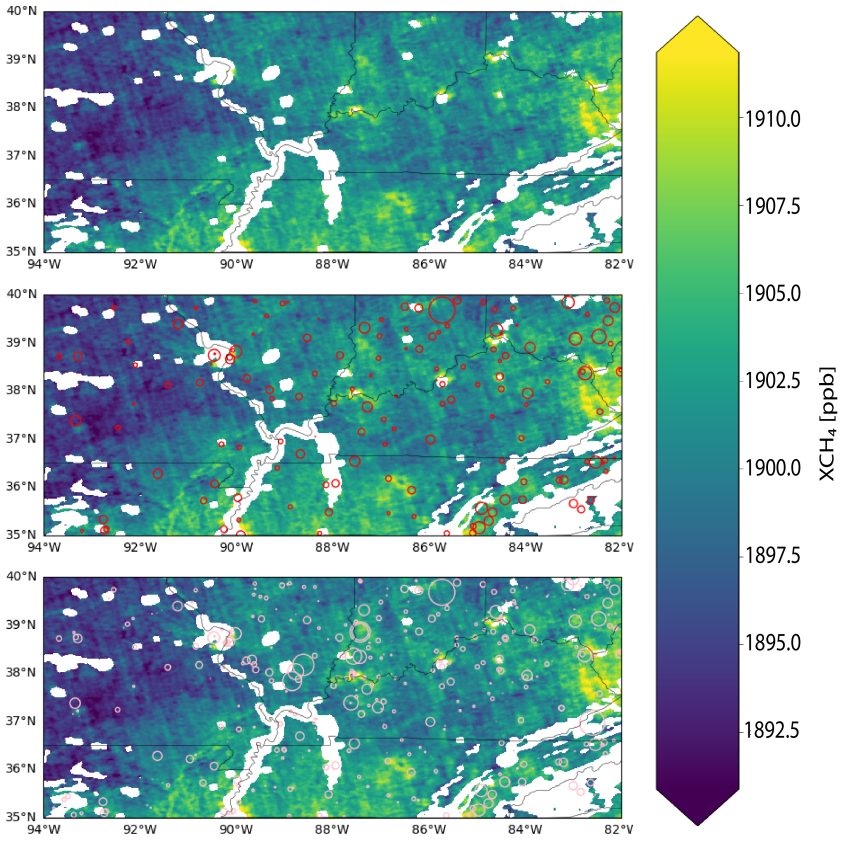

Figure 3.7: (top) Region around Laurel Ridge Landfill. (middle) Region around Laurel Ridge Landfill with landfills overlaid in red. (bottom) Region around Laurel Ridge Landfill with landfills overlaid in red and methane-emitting facilities in pink as identified by the EPA GHGRP. The size of the red and pink circles is proportional to the methane emissions reported by the GHGRP. All data is for 2022.

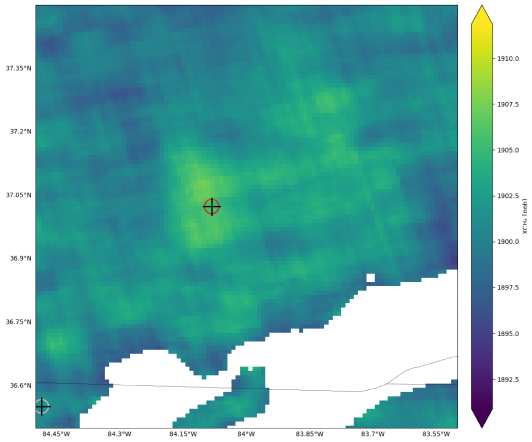

Figure 3.8: Laurel Ridge landfill is marked by the crosshair with a red circle. Other facilities as identified by the GHGRP are crosshairs with a pink circle.

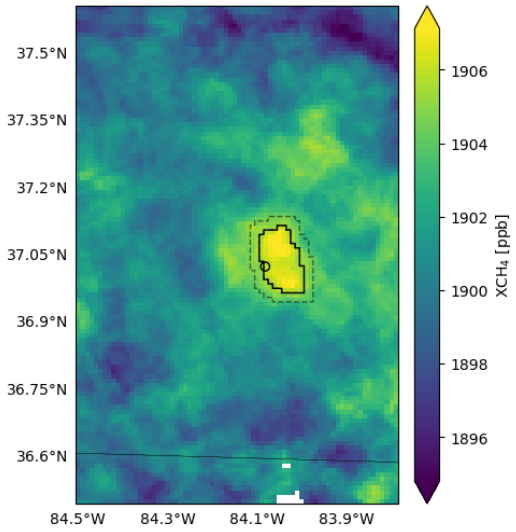

Figure 3.9: Laurel Ridge Landfill wind-rotated using 2022 data. Laurel Ridge Landfill is marked with a black circle. The plume is defined as the area inside the solid black line which has a methane concentration above the 98.5 percentile compared to the background. The background methane concentration is determined by the area between the solid black line and the dashed black line, here having a width of two grid cells.

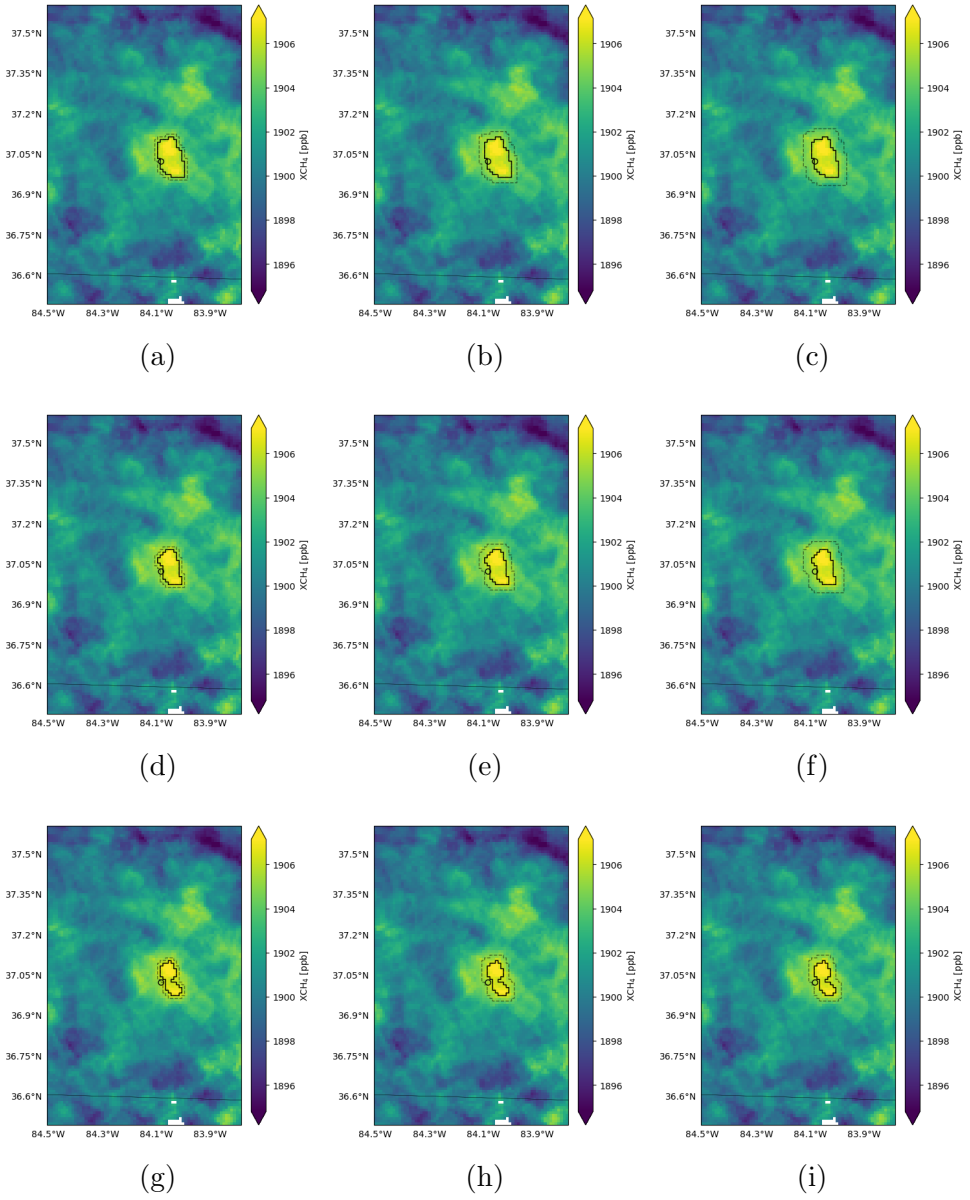

Figure 3.10: Oversampled region, wind-rotated around Laurel Ridge Landfill using 2022 data. Oversampled at 0.01°x 00.1°resolution. The solid black line delineates a plume. Laurel Ridge Landfill is marked with a black circle. The area between the dashed black line and the solid black line is considered the background. The plume is defined as the region above the (a-c) 98.5, (d-f) 99, or (g-i) 99.25 percentile. The background has a cell width beyond the plume perimeter of (a, d, g) 1 cell, (b, e, h) 2 cells, or (c, f, i) 3 cells.

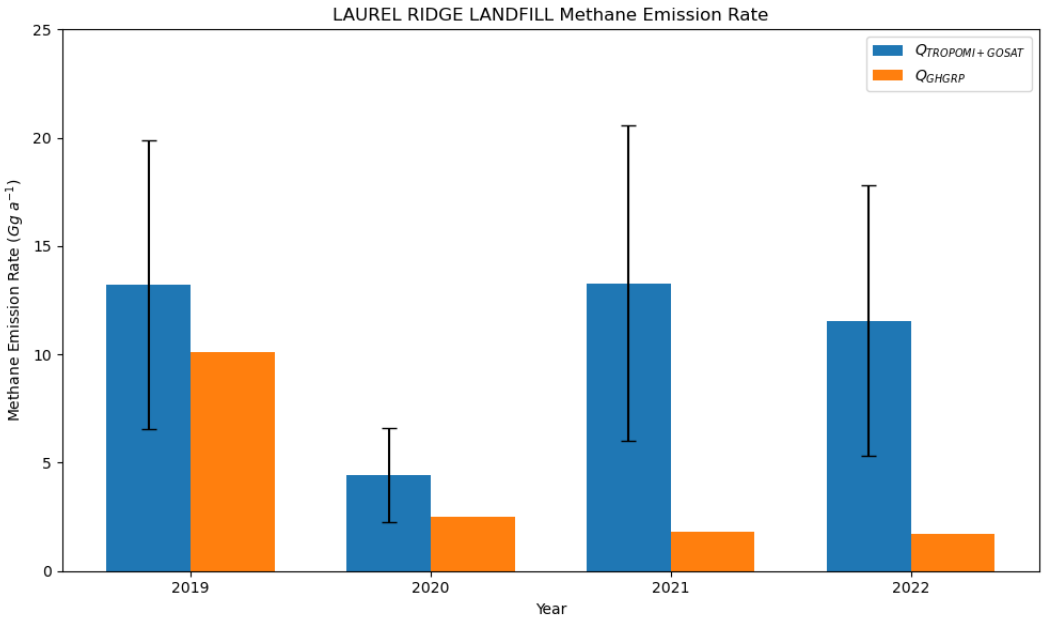

Figure 3.11: Laurel Ridge Landfill methane emission rate through time.

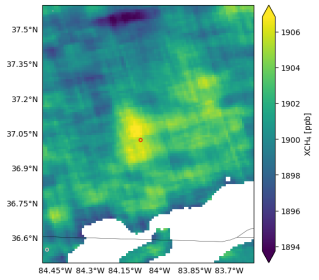

(a) Laurel Ridge Landfill

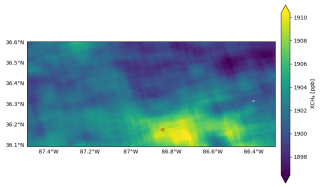

(b) Bordeaux Landfill

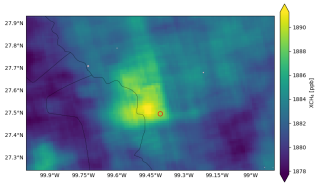

(c) City of Laredo Landfill

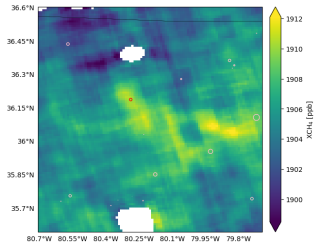

(d) Hanes Mill Road Landfill

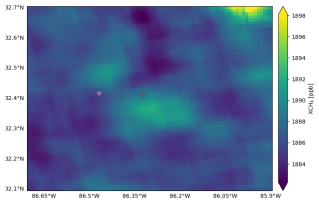

(e) Montgomery City of Landfill

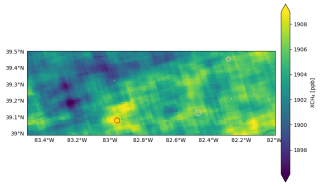

(f) Pike Sanitation Landfill

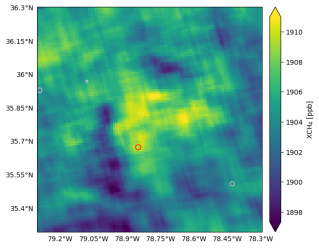

(g) South Wake Landfill

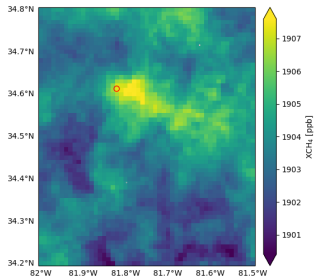

(h) Union County Landfill

Figure 3.12: Methane concentration maps in [ppb] for regions around different landfills (2022)

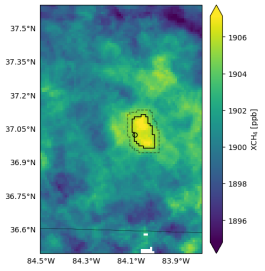

(a) Laurel Ridge Landfill wind rotated

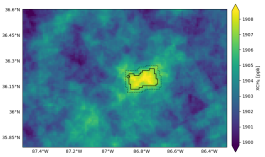

(b) Bordeaux Landfill wind rotated

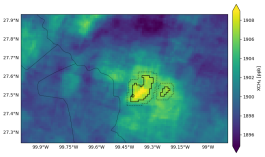

(c) City of Laredo Landfill wind rotated

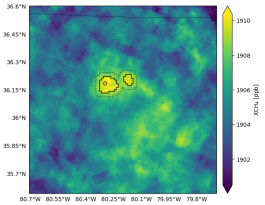

(d) Hanes Mill Road Landfill wind rotated

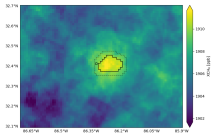

(e) Montgomery City of Landfill wind rotated

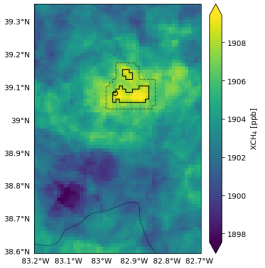

(f) Pike Sanitation Landfill wind rotated

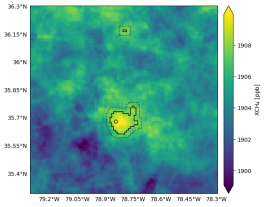

(g) South Wake Landfill wind rotated

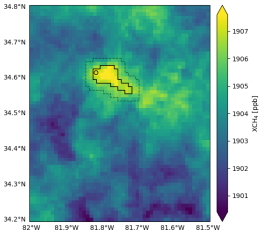

(h) Union County Landfill wind rotated

Figure 3.13: Wind-rotated methane concentration maps in [ppb] for different landfills (2022). Maps after wind rotation. A solid black line traces the perimeter of a methane plume. Landfills are marked with a black circle. The region between the solid black line and dashed black line has a width of two cells, and it is the region used to calculate the background methane concentration in these examples.

Table 3.4: CH_4 Emission Rates: GHGRP vs TROPOMI+GOSAT 2019.

	GHGRP ($Gg\,a^{-1}$)	TROPOMI+GOSAT ($Gg\,a^{-1}$)
SOUTH WAKE LANDFILL	3.91	8.31 ± 4.69
LAUREL RIDGE LANDFILL	10.09	13.21 ± 6.65
BORDEAUX LANDFILL	2.48	6.28 ± 3.15
CITY OF LAREDO LANDFILL	6.58	13.01 ± 4.82
UNION COUNTY REGIONAL MSW LANDFILL	5.67	8.09 ± 2.86

Table 3.5: CH_4 Emission Rates: GHGRP vs TROPOMI+GOSAT 2020.

	GHGRP ($Gg\,a^{-1}$)	TROPOMI+GOSAT ($Gg\,a^{-1}$)
LAUREL RIDGE LANDFILL	2.49	4.42 ± 2.16
BORDEAUX LANDFILL	2.42	11.34 ± 6.20
CITY OF LAREDO LANDFILL	6.80	15.75 ± 6.30
MONTGOMERY CITY OF LANDFILL	5.75	6.72 ± 4.43

Table 3.6: CH_4 Emission Rates: GHGRP vs TROPOMI+GOSAT 2021.

	GHGRP ($Gg\,a^{-1}$)	TROPOMI+GOSAT ($Gg\,a^{-1}$)
SOUTH WAKE LANDFILL	6.30	12.43 ± 4.46
LAUREL RIDGE LANDFILL	1.80	13.28 ± 7.27
BORDEAUX LANDFILL	2.36	9.55 ± 4.80
CITY OF LAREDO LANDFILL	6.97	14.46 ± 7.36
MONTGOMERY CITY OF LANDFILL	5.29	7.17 ± 4.50
UNION COUNTY REGIONAL MSW LANDFILL	4.11	3.77 ± 1.99

Table 3.7: CH_4 Emission Rates: GHGRP vs TROPOMI+GOSAT 2022.

	GHGRP ($Gg\,a^{-1}$)	TROPOMI+GOSAT ($Gg\,a^{-1}$)
SOUTH WAKE LANDFILL	5.96	14.38 ± 4.58
LAUREL RIDGE LANDFILL	1.70	11.56 ± 6.25
HANES MILL ROAD LANDFILL	1.58	8.33 ± 5.26
PIKE SANITATION INC	9.65	10.99 ± 3.70
BORDEAUX LANDFILL	2.11	15.60 ± 7.74
CITY OF LAREDO LANDFILL	7.14	15.97 ± 5.14
MONTGOMERY CITY OF LANDFILL	5.28	7.82 ± 4.75
UNION COUNTY REGIONAL MSW LANDFILL	4.87	6.53 ± 2.94

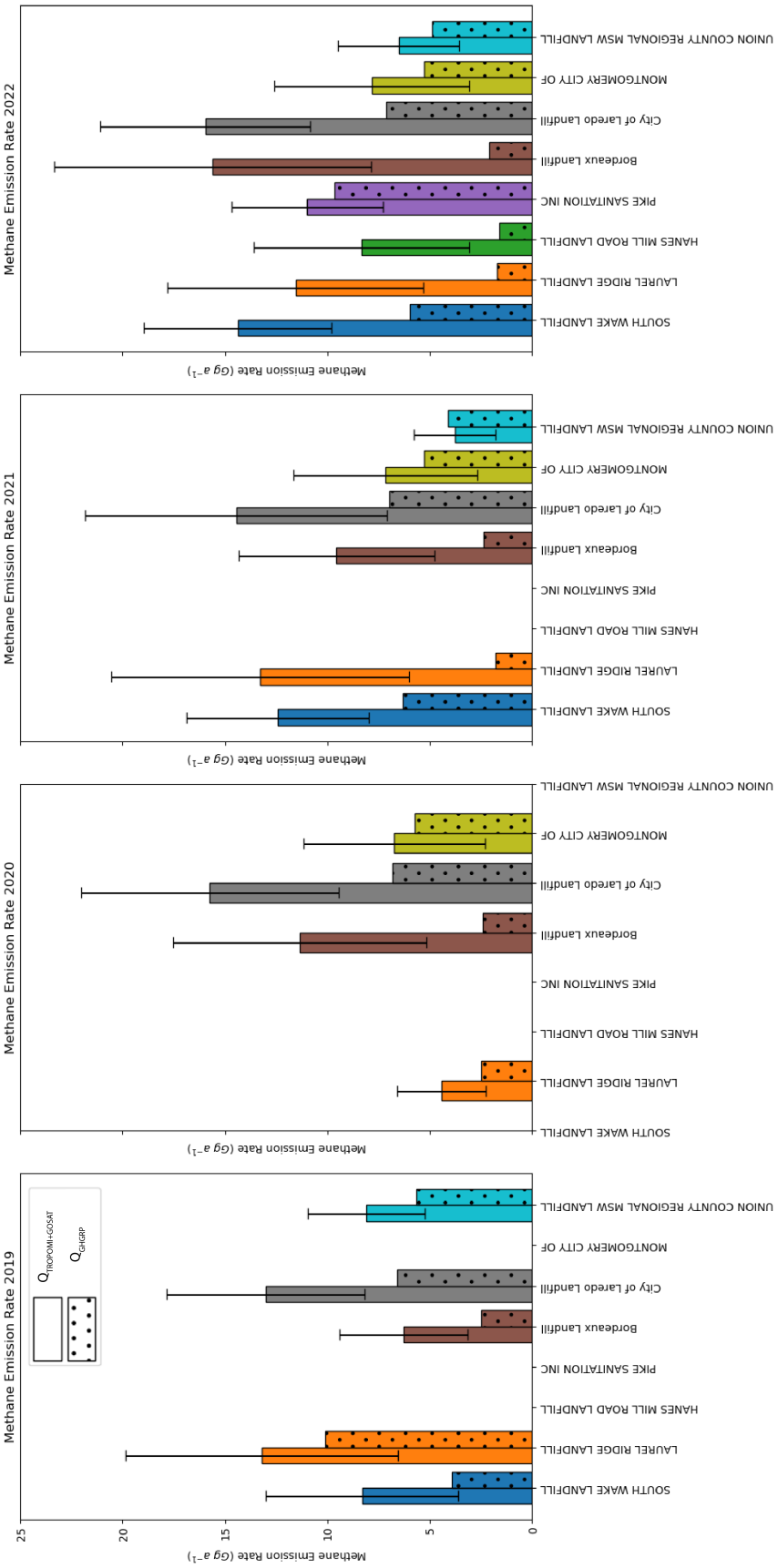

Figure 3.14: Methane emission rate through time for all landfills.

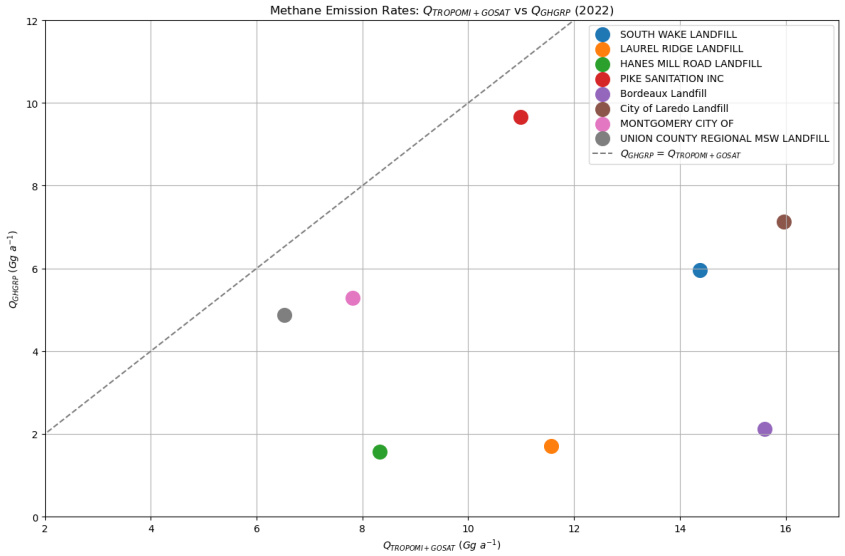

Figure 3.15: Methane emission rate GHGRP versus TROPOMI+GOSAT (2022).

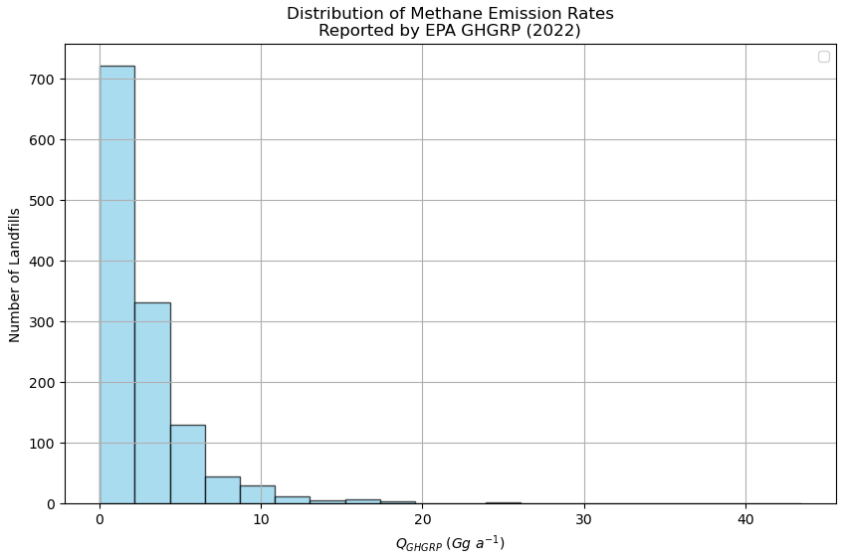

Figure 3.16: Distribution of methane emission rates reported by the GHGRP in 2022.

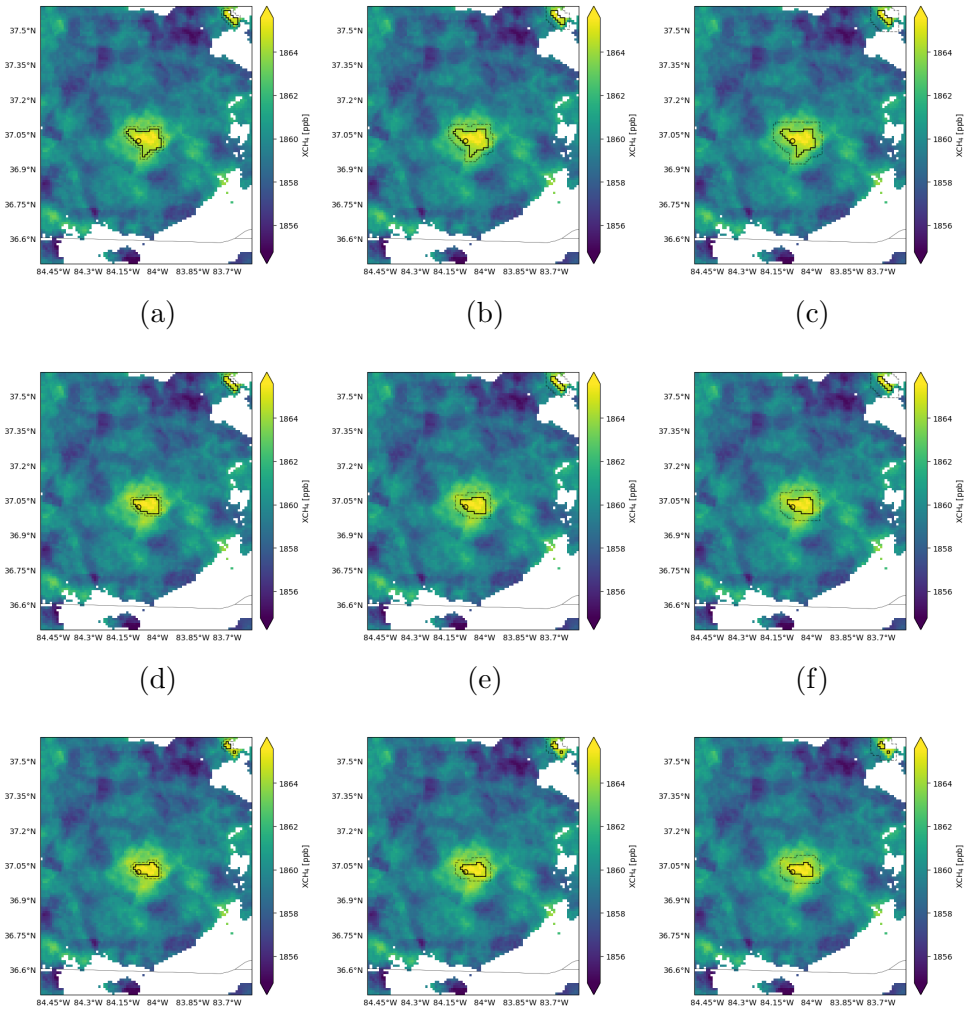

Figure 3.17: Oversampled region, wind-rotated around Laurel Ridge Landfill using 2019 data. Oversampled at 0.01°x 00.1°resolution. The solid black line delineates a plume. Laurel Ridge Landfill is marked with a black circle. The area between the dashed black line and the solid black line is considered the background. The plume is defined as the region above the (a-c) 98.5, (d-f) 99, or (g-i) 99.25 percentile. The background has a cell width beyond the plume perimeter of (a, d, g) 1 cell, (b, e, h) 2 cells, or (c, f, i) 3 cells.

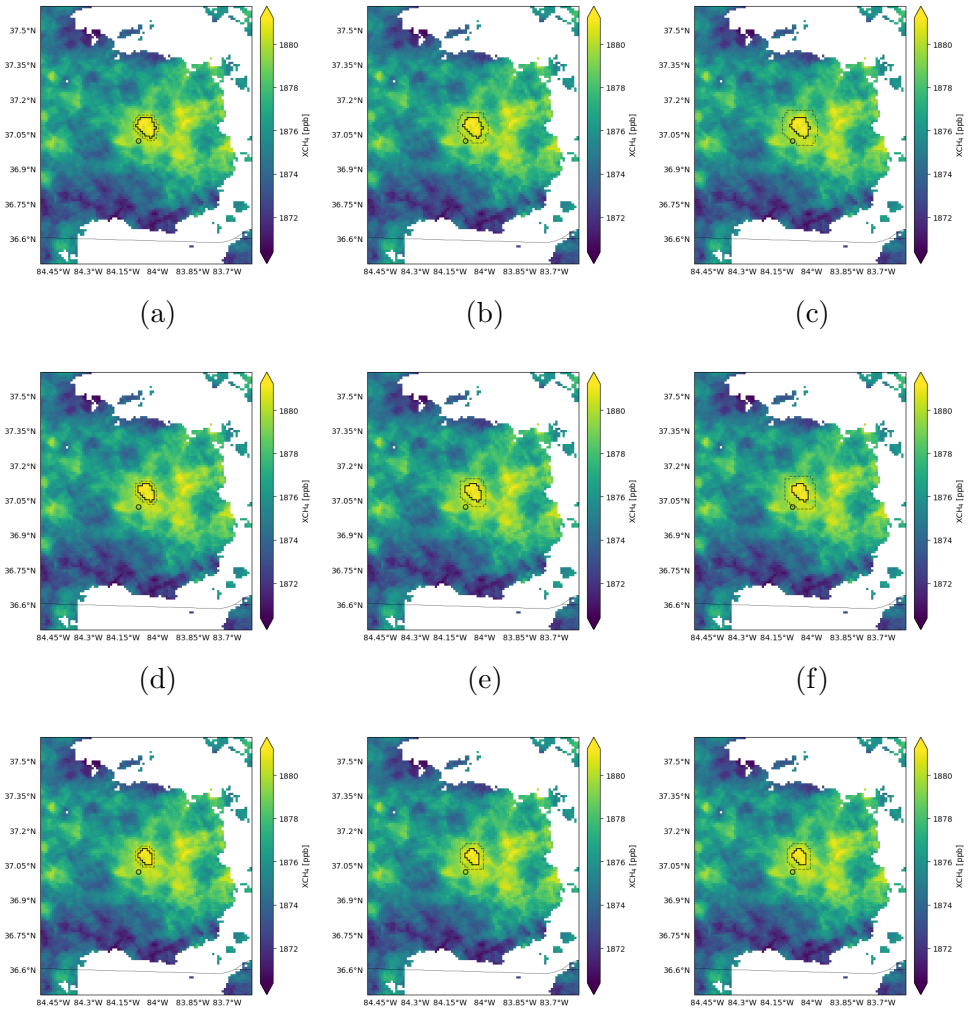

Figure 3.18: Oversampled region, wind-rotated around Laurel Ridge Landfill using 2020 data. Oversampled at 0.01°x 00.1°resolution. The solid black line delineates a plume. Laurel Ridge Landfill is marked with a black circle. The area between the dashed black line and the solid black line is considered the background. The plume is defined as the region above the (a-c) 98.5, (d-f) 99, or (g-i) 99.25 percentile. The background has a cell width beyond the plume perimeter of (a, d, g) 1 cell, (b, e, h) 2 cells, or (c, f, i) 3 cells.

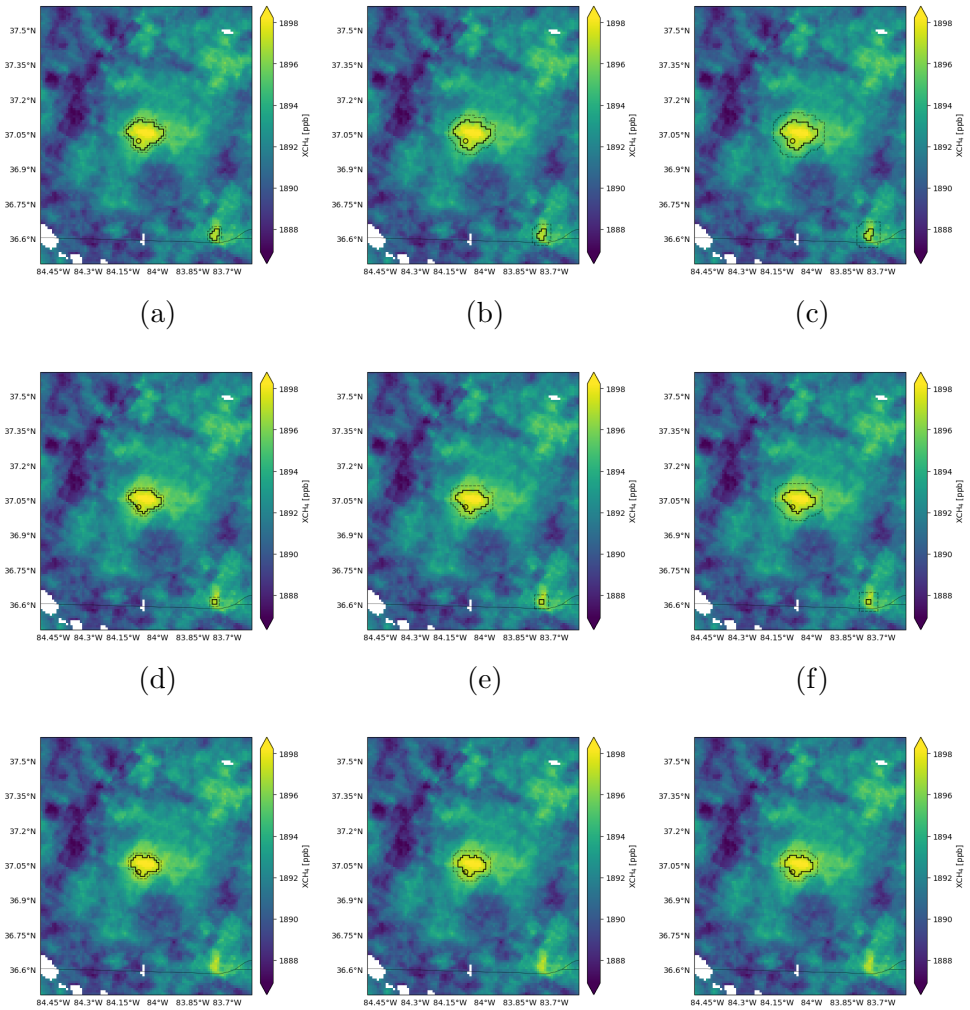

Figure 3.19: Oversampled region, wind-rotated around Laurel Ridge Landfill using 2021 data. Oversampled at 0.01°x 00.1°resolution. The solid black line delineates a plume. Laurel Ridge Landfill is marked with a black circle. The area between the dashed black line and the solid black line is considered the background. The plume is defined as the region above the (a-c) 98.5, (d-f) 99, or (g-i) 99.25 percentile. The background has a cell width beyond the plume perimeter of (a, d, g) 1 cell, (b, e, h) 2 cells, or (c, f, i) 3 cells.

Chapter 4

Discussion

4.1 Comparing Emissions

We evaluate differences in emissions as reported by the EPA GHGRP versus as calculated through oversampling of TROPOMI+GOSAT data. Table 3.3 and Figure 3.14 summarize this information, giving us insights into eight landfills.

4.1.1 Example Landfill: Laurel Ridge Landfill

We show the area containing Laurel Ridge Landfill region in Figure 3.7, demonstrating that the landfill is isolated from other methane-emitting facilities. In Figure 3.8, we can see only one other facility, which is distant from Laurel Ridge Landfill. Upon wind rotation and oversampling, we get plume structures pointing downwind as seen in Figure 3.10 with 2022 data. Varying the plume percentile between 98.5, 99, and 99.25 gave rise to reasonable plumes. It is difficult to ascertain what the background methane concentration looks like. In other words, we cannot be sure that taking a belt with cell width of one around the perimeter of the plume versus a cell width of three is better at describing background methane. These two parameters gave rise to nine combinations, where the lowest methane emission rate was 5.96 $\mathrm{Gg\,a^{-1}}$ with plume percentile of 99.25 and one background cell and the greatest was 18.45 $\mathrm{Gg\,a^{-1}}$ with plume percentile of 98.5 and three background cells. The GHGRP reports 1.70 Gg for 2022 for this landfill, which remains significantly

lower than our lowest estimate. Table 3.3 shows an annual comparison with a visualization in Figure 3.11.

The GHGRP reports a downward trend over the last four years in methane emissions for Laurel Ridge Landfill. We don't find a downward trend or a discernible trend through time at all. For each year, our method employing satellite data reports greater methane emissions. The gap between our emission estimates and the GHGRP estimates are widest in 2021 and 2022 for Laurel Ridge Landfill. Figures 3.17, 3.18, 3.19, 3.10 all show maps of the methane plumes we use to estimate emissions for Laurel Ridge Landfill. With the exception of 2020, all display reasonable methane plumes pointing downwind. While it is difficult to determine whether the plumes from the 2020 maps are reasonable for the IME method, we have chosen to include them but proceed with caution with analyses that make reference to Laurel Ridge Landfill in 2020.

4.1.2 Other Landfills

For South Wake Landfill, we do not have a characteristic plume structure for 2020, so we exclude 2020 from our analysis. For 2019, 2021, and 2022, there is a discrepancy between top-down and bottom-up estimates. This discrepancy is greatest in 2022, with an upward trend in both our top-down estimate and in emission discrepancy throughout the years.

We include only 2022 for Hanes Mill Road Landfill as this is the only year with a discernible plume structure.

In the context of our selected landfills in 2022, we see the greatest discrepancy in emission estimates for Bordeaux Landfill.

The EPA reports that Bordeaux Landfill is no longer open and that it accepted waste between 1973 and 1994. Since it began reporting data in 2010,

there is a reported downward trend in emissions (*US EPA*, 2022) which we do not observe in our estimates.

Pike Sanitation Inc. Landfill and Bordeaux Landfill are the only two landfills within our sample that report having passive vents and/or flares present. While both show a discrepancy between top-down and bottom-up estimates, this discrepancy is a lot smaller for Pike Sanitation Inc. Landfill.

A unique case is 2021 for Union County Regional MSW Landfill, where the GHGRP estimate was slightly higher than the oversampled satellite data estimate. The methane plume for this particular year for Union County Regional MSW Landfill was particularly difficult to determine, as can be seen in Figure 4.18. We have chosen to include this year since the plumes delineated by the plume masks look reasonable, but we are cautious about results for this particular year. This reveals a limitation of the methodology where we are unable to ascertain the contributions to a plume in cases with multiple plume structures like those in Figure 4.18.

4.1.3 Discrepancy Uncertainty

From Table 3.7, we can see that, although Pike Sanitation Inc. Landfill has a greater top-down than bottom-up estimate, the bottom-up estimate is still within the range of top-down uncertainty. This is also the case for each year's estimates for Montgomery City of Landfill and Union County Regional MSW Landfill. Thus, our results indicate greater evidence of an emissions discrepancy for South Wake Landfill, Laurel Ridge Landfill, Hanes Mill Road Landfill, Bordeaux Landfill, and City of Laredo Landfill.

4.2 Landfill Characteristics

The GHGRP reports landfill characteristics such as the total surface area that contains waste, the type of cover used by the landfill (clay, sand, etc.), the years of operation, and more (*US EPA*, 2022). Tables 4.1 and 4.2 summariaze these data.

Landfill	**Cover Type**	**Waste-Containing Surface Area** (m^2)	**Total Annual Waste Disposal (metric tons)**
SOUTH WAKE LANDFILL	clay; other soil mixture	376362.00	484683.4102
LAUREL RIDGE LANDFILL	clay	492548.20	366785.3300
HANES MILL ROAD LANDFILL	clay; other soil mixture	736536.00	244819.5170
PIKE SANITATION INC	other soil mixture	310148.00	365499.0000
BORDEAUX LANDFILL	clay	768828.00	NaN
CITY OF LAREDO LANDFILL	clay	609868.00	367622.1046
MONTGOMERY CITY OF	other soil mixture	221712.73	133573.6500
UNION COUNTY REGIONAL MSW LANDFILL	clay; organic; sand	441112.00	704077.7701

Table 4.1: GHGRP data for selected landfills Part 1

Landfill	**Landfill Open?**	**Gas Collection System?**	**Passive Vents and Flares?**
SOUTH WAKE LANDFILL	Y	Y	N
LAUREL RIDGE LANDFILL	Y	Y	N
HANES MILL ROAD LANDFILL	Y	Y	N
PIKE SANITATION INC	Y	Y	Y
BORDEAUX LANDFILL	N	Y	Y
CITY OF LAREDO LANDFILL	Y	Y	N
MONTGOMERY CITY OF	Y	Y	N
UNION COUNTY REGIONAL MSW LANDFILL	Y	Y	N

Table 4.2: GHGRP data for selected landfills Part 2

We show a correlation heatmap in Figure 4.1 using the data on these landfill characteristics in relation to our methane emission estimates.

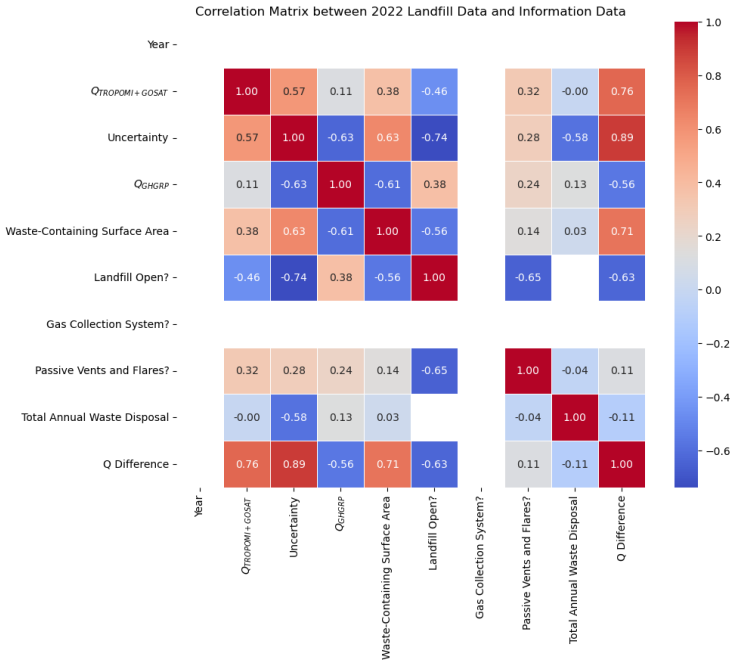

Figure 4.1: Emission Rate and Landfill Information Correlation Heatmap 2022. $Q_{TROPOMI+GOSAT}$ refers to the methane emission rate calculated through our oversampling procedure. Q_{GHGRP} is the methane emission rate reported by the EPA GHGRP. Q Difference refers to the $Q_{TROPOMI+GOSAT} - Q_{GHGRP}$. All landfills report having a gas collection system, removing the correlation coefficients of this variable with other variables.

Some interesting correlations arise out of the relationship of some variables with the emission estimates discrepancies; in other words, with the differences "Q Difference" between our emissions estimates and the GHGRP estimates. Its correlation coefficient of -0.63 with "Landfill Open?" can be explained by the fact that only Bordeaux Landfill is not an open landfill, and Bordeaux Landfill has the greatest emissions estimate discrepancy. The correlation between the emissions discrepancy and the Waste-Containing Surface Area stands out, having a coefficient of 0.71. Figure 4.2 indicates a direct positive relationship between these two variables. For our sample of landfills, we may then expect landfills with greater waste-containing areas to experience the most under-reported emissions. However, we cannot assert that this relationship holds for the larger population of landfills since we have a small sample size of eight.

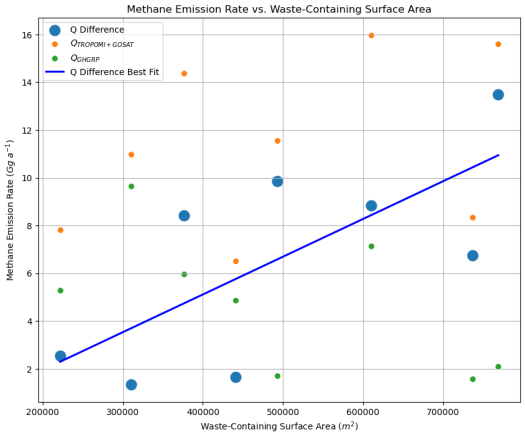

Figure 4.2: Waste-containing surface area versus methane emission rate 2022.

Another interesting relationship arises between the methane emission rate discrepancy and cover type. With a correlation coefficient of -0.73, we can visualize the relationship via Figure 4.3. The landfills with the greatest emissions discrepancies all use clay covers or a combination of clay covers and other soil mixture. Landfill covers serve multiple purposes, with one of them

being a reduction of methane emissions. With help from methanotrophic bacteria, CH_4 can be oxidized to CO_2 (*Hanson and Hanson*, 1996; *Bowman*, 2006; *Bürgmann*, 2011; *Sadasivam and Reddy*, 2014) in landfill soil covers. A challenge with soil covers is their long-term degradation (*Sadasivam and Reddy*, 2014; *Chetri and Reddy*, 2021). At the same time, clay covers, owing to their low permeability, may provide better protection against infiltration and prevent greater landfill gas emissions (*Chetri and Reddy*, 2021). These factors, along with the upfront and maintenance costs of landfill covers, are likely considerations for landfill operators. The GHGRP requires reporting of a methane oxidation fraction (*US EPA*, 2014). For reporting before 2013, this fraction can be taken as 0.10 regardless of cover type. After 2013, the fraction varies depending on the type of cover employed by the landfill. Landfill covers also affect the Landfill Gas Collection Efficiency reported. Based on our results, it may then be important to reconsider the values of these parameters from the GHGRP to lower the discrepancies we see for certain cover types.

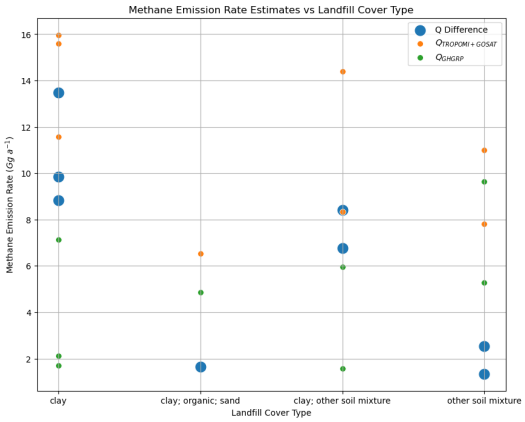

Figure 4.3: Methane emission rate versus cover type 2022

4.3 Limitations

The analysis for this project is limited geographically due to several factors. The HRRR weather model provides wind data for North America (*Dowell et al.*, 2022), and the EPA GHGRP provides reports for facilities in the United States. Expanding this project to landfills outside the United States would then require different data sources.

Another geographical constraint arises from poor data density. This was mainly present in the western United States, the Florida region, and the north-eastern United States. We saw that the data density improves for Florida and the northeast when including data from four years (2019-2022), as is visible when comparing Figure 3.1 and Figure 3.3. The poor data density after over-sampling is due to several factors including our filter that removes coastal and low-data quality observations. We also require that, in order to preserve the information content of the original data, our oversampled grid cells at 0.01°x 0.01°resolution contain at least 40 observations.

We can see that most landfills selected for the project are located in the southeastern portion of the United States in Figure 4.4. This then limits our ability to compare one region to another. Assuming that there are no regional differences in bottom-up landfill methane reporting, we suggest that they are being under-reported. This under-reporting is with reference to our top-down estimates employing TROPOMI+GOSAT data.

Many landfills were excluded from the analysis because they are too close in proximity to other landfills or to other methane-emitting facilities. This proximity poses a problem because it is difficult to distinguish the methane emissions that are due to the landfill from those due to other sources. On the other hand, if we see a characteristic downwind plume arise from wind

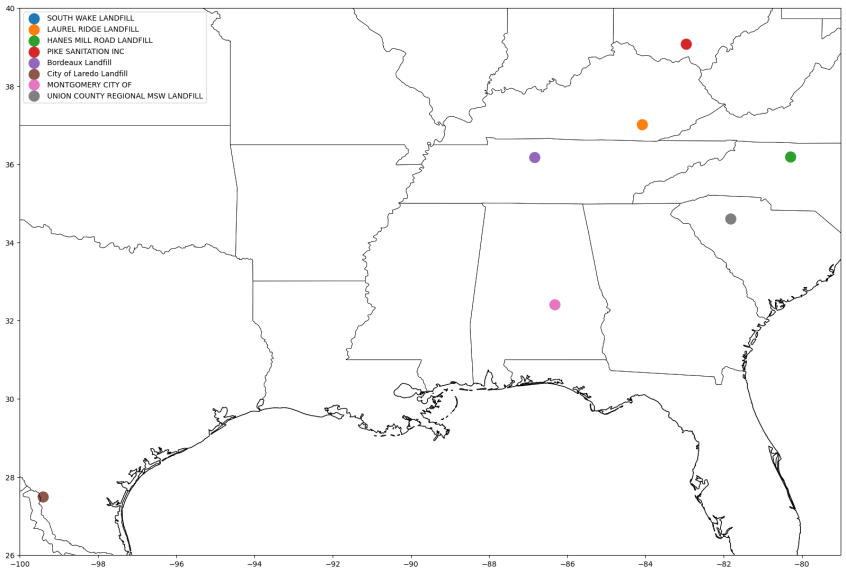

Figure 4.4: Landfill locations across the United States.

rotation followed by oversampling from an isolated landfill, we can be more certain that the methane enhancements from the plume are due to the landfill. Our method of oversampling allows us to access a very fine spatial resolution and therefore gain an understanding of methane concentrations above a specific landfills. However, the fine resolution of methane concentrations is limited in information since we need to know, through our wind-rotation method, the source of the methane concentrations.

4.3.1 Future Directions

The project can evolve in different ways, all providing valuable information to both supplement the results relevant to this project and to explore new avenues.

With our methodology, it is likely possible to identify more landfills that give rise to methane plume structures where an IME quantification method is reasonable. These landfills would still only be within areas with sufficient data density and with landfills that are isolated from other methane-emitting

facilities. Hence, an interesting addition to this project would be one that can filter out other methane-emitting facilities. A way that this could be explored is with data on gases not commonly emitted by landfills. Understanding the plume structure of this additional gas can help us attribute the methane plume to either one of the facilities. A challenge with this approach is the case where two landfills are in proximity to each other.

It would also be interesting to further explore the landfills by characteristic; that is, by analyzing landfills as subsets based on whether they use a specific type of cover, their waste-containing surface area, etc. This would help us understand more of the underlying causes of the emissions discrepancies we observe and help us determine whether discrepancies are systematic or isolated incidents.

4.4 Conclusions

For nearly all of the selected landfills, our results suggest a discrepancy between the bottom-up and top-down methane emission estimates, where top-down estimates are greater than the bottom-up ones. For South Wake Landfill, Laurel Ridge Landfill, Bordeaux Landfill, City of Laredo Landfill, and Montgomery City of Landfill, we find the greatest emission discrepancy in 2022. From Table 3.7, we can see that, for the eight landfills, the lowest discrepancy is for Pike Sanitation Inc. Landfill which, without considering the uncertainty in the top-down estimate, underestimates its emissions by 1.34 $\mathrm{Gg\,a^{-1}}$ in its bottom-up estimate. The greatest discrepancy is 13.49 $\mathrm{Gg\,a^{-1}}$, coming from Bordeaux Landfill.

From Figure 3.15 and Figure 3.16, we can see that the selected landfills have greater methane emissions than most landfills reported by the GHGRP. Their

methane emission reports, and likewise discrepancies in emission estimates, thus carry significant weight.

4.5 Implications

A major goal of top-down methane emission estimates is to inform bottom-up estimates. We do observe discrepancies in the two types of reports, suggesting a reconsideration of the parameters employed in bottom-up calculations.

Our analysis included one landfill, Bordeaux Landfill, that is closed for operations and seven others that remain open. Bordeaux landfill shows the greatest emissions discrepancies, suggesting a possible issue of under-reporting due to a lack of upkeep or updating in emissions reporting.

Landfills including South Wake Landfill, Laurel Ridge Landfill, and Union County Regional MSW Landfill have proposed projects turning landfill methane gas into renewable energy (*Wake County*, 2022; *December 15 and 2022*; *Bruns*). Hanes Mill Road Landfill also reports methane capture and destruction as well as conversion to electrical energy (*City of Winston-Salem Office of Sustainability*, 2021; *Peplowski*) With the increase in renewable energy projects as well as the development of technologies concerning methane, it remains important to quantify landfill methane emissions in order to accurately quantify the impact of landfill projects. Likewise, top-down estimates remain important to verify bottom-up reports.

There are landfills that are located in proximity to human communities, and in some cases disproportionately under-resourced, minority, and/or vulnerable communities, raising environmental justice issues. For instance, Bordeaux Landfill sits in a historically black neighborhood that closed after public protest (*Wadhwani et al.*, 2022). However, we observe that Bordeaux Landfill

continues to emit methane, and at rates greater than reported through the GHGRP.

Ultimately, a more informed parameterization of bottom-up landfill estimates would enable more accurate methane quantification and consequently a better understanding of methane sector contributions. Knowing how much landfills as a sector contribute to the national methane budget can inform policy and resource allocation. In the context of climate change, accurate methane quantification, in conjunction with accurate reporting of other greenhouse gases, allows for better monitoring of changes through time and better measurements like health and economic outcomes that often inform policy and agreements at the local and global levels.

References

Aben, I., O. Hasekamp, and W. Hartmann (2007), Uncertainties in the space-based measurements of CO2 columns due to scattering in the Earth's atmosphere, *Journal of Quantitative Spectroscopy and Radiative Transfer*, *104*(3), 450–459, doi:10.1016/j.jqsrt.2006.09.013.

ATSDR (2001), Chapter 2: Landfill Gas Basics.

Balasus, N., D. J. Jacob, A. Lorente, J. D. Maasakkers, R. J. Parker, H. Boesch, Z. Chen, M. M. Kelp, H. Nesser, and D. J. Varon (2023), A blended TROPOMI+GOSAT satellite data product for atmospheric methane using machine learning to correct retrieval biases, *Atmospheric Measurement Techniques*, *16*(16), 3787–3807, doi:10.5194/amt-16-3787-2023, publisher: Copernicus GmbH.

Beirle, S., K. F. Boersma, U. Platt, M. G. Lawrence, and T. Wagner (2011), Megacity Emissions and Lifetimes of Nitrogen Oxides Probed from Space, *Science*, *333*(6050), 1737–1739, doi:10.1126/science.1207824, publisher: American Association for the Advancement of Science.

Bowman, J. (2006), The Methanotrophs — The Families Methylococcaceae and Methylocystaceae, in *The Prokaryotes: Volume 5: Proteobacteria: Alpha and Beta Subclasses*, edited by M. Dworkin, S. Falkow, E. Rosenberg, K.-H. Schleifer, and E. Stackebrandt, pp. 266–289, Springer, New York, NY, doi:10.1007/0-387-30745-1_15.

Bruns, A. (), Waste to Energy: Slow Burn || Site Selection Online.

Butz, A., O. P. Hasekamp, C. Frankenberg, J. Vidot, and I. Aben (2010), CH4 retrievals from space-based solar backscatter measurements: Performance evaluation against simulated aerosol and cirrus loaded scenes, *Journal of Geophysical Research: Atmospheres*, *115*(D24), doi:10.1029/2010JD014514, _eprint: https://onlinelibrary.wiley.com/doi/pdf/10.1029/2010JD014514.

Butz, A., A. Galli, O. Hasekamp, J. Landgraf, P. Tol, and I. Aben (2012), TROPOMI aboard Sentinel-5 Precursor: Prospective performance of CH4

retrievals for aerosol and cirrus loaded atmospheres, *Remote Sensing of Environment*, *120*, 267–276, doi:10.1016/j.rse.2011.05.030.

Bürgmann, H. (2011), Methane Oxidation (Aerobic), in *Encyclopedia of Geobiology*, edited by J. Reitner and V. Thiel, Encyclopedia of Earth Sciences Series, pp. 575–578, Springer Netherlands, Dordrecht, doi:10.1007/978-1-4020-9212-1_139.

Chetri, J. K., and K. R. Reddy (2021), Advancements in Municipal Solid Waste Landfill Cover System: A Review, *Journal of the Indian Institute of Science*, *101*(4), 557–588, doi:10.1007/s41745-021-00229-1.

City of Winston-Salem Office of Sustainability (2021), City of Winston-Salem Community Greenhouse Gas Emissions Inventory and Energy Report, *Tech. rep.*, CITY OF WINSTON-SALEM.

de Foy, B., Z. Lu, D. G. Streets, L. N. Lamsal, and B. N. Duncan (2015), Estimates of power plant NOx emissions and lifetimes from OMI NO2 satellite retrievals, *Atmospheric Environment*, *116*, 1–11, doi:10.1016/j.atmosenv.2015.05.056.

December 15, B. G. |., and 2022 (), Vision RNG, Waste Connections partner on Laurel Ridge Landfill RNG project.

Dowell, D. C., C. R. Alexander, E. P. James, S. S. Weygandt, S. G. Benjamin, G. S. Manikin, B. T. Blake, J. M. Brown, J. B. Olson, M. Hu, T. G. Smirnova, T. Ladwig, J. S. Kenyon, R. Ahmadov, D. D. Turner, J. D. Duda, and T. I. Alcott (2022), The High-Resolution Rapid Refresh (HRRR): An Hourly Updating Convection-Allowing Forecast Model. Part I: Motivation and System Description, *Weather and Forecasting*, *37*(8), 1371–1395, doi:10.1175/WAF-D-21-0151.1.

Fioletov, V. E., C. A. McLinden, N. Krotkov, C. Li, J. Joiner, N. Theys, S. Carn, and M. D. Moran (2016), A global catalogue of large SO_2 sources and emissions derived from the Ozone Monitoring Instrument, *Atmospheric Chemistry and Physics*, *16*(18), 11,497–11,519, doi:10.5194/acp-16-11497-2016, publisher: Copernicus GmbH.

Frankenberg, C., A. K. Thorpe, D. R. Thompson, G. Hulley, E. A. Kort, N. Vance, J. Borchardt, T. Krings, K. Gerilowski, C. Sweeney, S. Con-

ley, B. D. Bue, A. D. Aubrey, S. Hook, and R. O. Green (2016), Airborne methane remote measurements reveal heavy-tail flux distribution in Four Corners region, *Proceedings of the National Academy of Sciences*, *113*(35), 9734–9739, doi:10.1073/pnas.1605617113, publisher: Proceedings of the National Academy of Sciences.

Hanson, R. S., and T. E. Hanson (1996), Methanotrophic bacteria, *Microbiological Reviews*, *60*(2), 439–471, doi:10.1128/mr.60.2.439-471.1996.

IPCC (2019), *2019 Refinement to the 2006 IPCC Guidelines for National Greenhouse Gas Inventories — IPCC*, IPCC, Switzerland, edited by: Calvo Buendia, E., Tanabe, K., Kranjc, A., Jamsranjav, B., Fukuda, M., Ngarize, S., Osako, A., Pyrozhenko, Y., Shermanau, P., and Federici, S.

Jacob, D. J., A. J. Turner, J. D. Maasakkers, J. Sheng, K. Sun, X. Liu, K. Chance, I. Aben, J. McKeever, and C. Frankenberg (2016), Satellite observations of atmospheric methane and their value for quantifying methane emissions, *Atmospheric Chemistry and Physics*, *16*(22), 14,371–14,396, doi:10.5194/acp-16-14371-2016, publisher: Copernicus GmbH.

Jongaramrungruang, S., G. Matheou, A. K. Thorpe, Z.-C. Zeng, and C. Frankenberg (2021), Remote sensing of methane plumes: instrument tradeoff analysis for detecting and quantifying local sources at global scale, *Atmospheric Measurement Techniques*, *14*(12), 7999–8017, doi:10.5194/amt-14-7999-2021, publisher: Copernicus GmbH.

Lorente, A., T. Borsdorff, A. Butz, O. Hasekamp, J. aan de Brugh, A. Schneider, L. Wu, F. Hase, R. Kivi, D. Wunch, D. F. Pollard, K. Shiomi, N. M. Deutscher, V. A. Velazco, C. M. Roehl, P. O. Wennberg, T. Warneke, and J. Landgraf (2021), Methane retrieved from TROPOMI: improvement of the data product and validation of the first 2 years of measurements, *Atmospheric Measurement Techniques*, *14*(1), 665–684, doi:10.5194/amt-14-665-2021, publisher: Copernicus GmbH.

Lu, Z., D. G. Streets, B. de Foy, L. N. Lamsal, B. N. Duncan, and J. Xing (2015), Emissions of nitrogen oxides from US urban areas: estimation from Ozone Monitoring Instrument retrievals for 2005–2014, *Atmospheric Chemistry and Physics*, *15*(18), 10,367–10,383, doi:10.5194/acp-15-10367-2015, publisher: Copernicus GmbH.

Myhre, G., D. Shindell, F.-M. Bréon, W. Collins, J. Fuglestvedt, J. Huang, D. Koch, J.-F. Lamarque, D. Lee, B. Mendoza, T. Nakajima, A. Robock, G. Stephens, H. Zhang, B. Aamaas, O. Boucher, S. B. Dalsøren, J. S. Daniel, P. Forster, C. Granier, J. Haigh, Hodnebrog, J. O. Kaplan, G. Marston, C. J. Nielsen, B. C. O'Neill, G. P. Peters, J. Pongratz, V. Ramaswamy, R. Roth, L. Rotstayn, S. J. Smith, D. Stevenson, J.-P. Vernier, O. Wild, P. Young, D. Jacob, A. R. Ravishankara, and K. Shine (2013), 8 Anthropogenic and Natural Radiative Forcing.

Nesser, H., D. J. Jacob, J. D. Maasakkers, A. Lorente, Z. Chen, X. Lu, L. Shen, Z. Qu, M. P. Sulprizio, M. Winter, S. Ma, A. A. Bloom, J. R. Worden, R. N. Stavins, and C. A. Randles (2023), High-resolution U.S. methane emissions inferred from an inversion of 2019 TROPOMI satellite data: contributions from individual states, urban areas, and landfills, *preprint*, Gases/Atmospheric Modelling and Data Analysis/Troposphere/Chemistry (chemical composition and reactions), doi:10.5194/egusphere-2023-946.

Parker, R., H. Boesch, A. Cogan, A. Fraser, L. Feng, P. I. Palmer, J. Messerschmidt, N. Deutscher, D. W. T. Griffith, J. Notholt, P. O. Wennberg, and D. Wunch (2011), Methane observations from the Greenhouse Gases Observing SATellite: Comparison to ground-based TCCON data and model calculations, *Geophysical Research Letters*, *38*(15), doi:10.1029/2011GL047871, _eprint: https://onlinelibrary.wiley.com/doi/pdf/10.1029/2011GL047871.

Parker, R. J., A. Webb, H. Boesch, P. Somkuti, R. Barrio Guillo, A. Di Noia, N. Kalaitzi, J. S. Anand, P. Bergamaschi, F. Chevallier, P. I. Palmer, L. Feng, N. M. Deutscher, D. G. Feist, D. W. T. Griffith, F. Hase, R. Kivi, I. Morino, J. Notholt, Y.-S. Oh, H. Ohyama, C. Petri, D. F. Pollard, C. Roehl, M. K. Sha, K. Shiomi, K. Strong, R. Sussmann, Y. Té, V. A. Velazco, T. Warneke, P. O. Wennberg, and D. Wunch (2020), A decade of GOSAT Proxy satellite CH_4 observations, *Earth System Science Data*, *12*(4), 3383–3412, doi:10.5194/essd-12-3383-2020, publisher: Copernicus GmbH.

Peplowski, H. C. (), CLIMATE ACTION PLAN.

Pommier, M., C. A. McLinden, and M. Deeter (2013), Relative changes in CO emissions over megacities based on observations from space, *Geophys-*

ical Research Letters, *40*(14), 3766–3771, doi:10.1002/grl.50704, _eprint: https://onlinelibrary.wiley.com/doi/pdf/10.1002/grl.50704.

Prather, M. J., C. D. Holmes, and J. Hsu (2012), Reactive greenhouse gas scenarios: Systematic exploration of uncertainties and the role of atmospheric chemistry, *Geophysical Research Letters*, *39*(9), doi:10.1029/2012GL051440, _eprint: https://onlinelibrary.wiley.com/doi/pdf/10.1029/2012GL051440.

Sadasivam, B. Y., and K. R. Reddy (2014), Landfill methane oxidation in soil and bio-based cover systems: a review, *Reviews in Environmental Science and Bio/Technology*, *13*(1), 79–107, doi:10.1007/s11157-013-9325-z.

Saunois, M., A. R. Stavert, B. Poulter, P. Bousquet, J. G. Canadell, R. B. Jackson, P. A. Raymond, E. J. Dlugokencky, S. Houweling, P. K. Patra, P. Ciais, V. K. Arora, D. Bastviken, P. Bergamaschi, D. R. Blake, G. Brailsford, L. Bruhwiler, K. M. Carlson, M. Carrol, S. Castaldi, N. Chandra, C. Crevoisier, P. M. Crill, K. Covey, C. L. Curry, G. Etiope, C. Frankenberg, N. Gedney, M. I. Hegglin, L. Höglund-Isaksson, G. Hugelius, M. Ishizawa, A. Ito, G. Janssens-Maenhout, K. M. Jensen, F. Joos, T. Kleinen, P. B. Krummel, R. L. Langenfelds, G. G. Laruelle, L. Liu, T. Machida, S. Maksyutov, K. C. McDonald, J. McNorton, P. A. Miller, J. R. Melton, I. Morino, J. Müller, F. Murguia-Flores, V. Naik, Y. Niwa, S. Noce, S. O'Doherty, R. J. Parker, C. Peng, S. Peng, G. P. Peters, C. Prigent, R. Prinn, M. Ramonet, P. Regnier, W. J. Riley, J. A. Rosentreter, A. Segers, I. J. Simpson, H. Shi, S. J. Smith, L. P. Steele, B. F. Thornton, H. Tian, Y. Tohjima, F. N. Tubiello, A. Tsuruta, N. Viovy, A. Voulgarakis, T. S. Weber, M. van Weele, G. R. van der Werf, R. F. Weiss, D. Worthy, D. Wunch, Y. Yin, Y. Yoshida, W. Zhang, Z. Zhang, Y. Zhao, B. Zheng, Q. Zhu, Q. Zhu, and Q. Zhuang (2020), The Global Methane Budget 2000–2017, *Earth System Science Data*, *12*(3), 1561–1623, doi:10.5194/essd-12-1561-2020, publisher: Copernicus GmbH.

Schepers, D., S. Guerlet, A. Butz, J. Landgraf, C. Frankenberg, O. Hasekamp, J.-F. Blavier, N. M. Deutscher, D. W. T. Griffith, F. Hase, E. Kyro, I. Morino, V. Sherlock, R. Sussmann, and I. Aben (2012), Methane retrievals from Greenhouse Gases Observing Satellite (GOSAT) shortwave infrared measurements: Performance comparison of proxy and physics retrieval algorithms, *Journal of Geophysical*

Research: Atmospheres, *117*(D10), doi:10.1029/2012JD017549, _eprint: https://onlinelibrary.wiley.com/doi/pdf/10.1029/2012JD017549.

Sun, K., L. Zhu, K. Cady-Pereira, C. Chan Miller, K. Chance, L. Clarisse, P.-F. Coheur, G. González Abad, G. Huang, X. Liu, M. Van Damme, K. Yang, and M. Zondlo (2018), A physics-based approach to oversample multi-satellite, multispecies observations to a common grid, *Atmospheric Measurement Techniques*, *11*(12), 6679–6701, doi:10.5194/amt-11-6679-2018, publisher: Copernicus GmbH.

US EPA (2014), Learn About the Greenhouse Gas Reporting Program (GHGRP).

US EPA (2016a), Municipal Solid Waste Landfills.

US EPA (2016b), Frequent Questions about Landfill Gas.

US EPA (2022), EPA GHGRP: Facility Level Information on GreenHouse Gases Tool (FLIGHT).

US EPA (2024), Draft Inventory of U.S. Greenhouse Gas Emissions and Sinks: 1990-2022.

Valin, L. C., A. R. Russell, and R. C. Cohen (2013), Variations of OH radical in an urban plume inferred from NO2 column measurements, *Geophysical Research Letters*, *40*(9), 1856–1860, doi:10.1002/grl.50267, _eprint: https://onlinelibrary.wiley.com/doi/pdf/10.1002/grl.50267.

Varon, D. J., D. J. Jacob, J. McKeever, D. Jervis, B. O. A. Durak, Y. Xia, and Y. Huang (2018), Quantifying methane point sources from fine-scale satellite observations of atmospheric methane plumes, *Atmospheric Measurement Techniques*, *11*(10), 5673–5686, doi:10.5194/amt-11-5673-2018, publisher: Copernicus GmbH.

Wadhwani, A., T. L. January 12, and 2022 (2022), Fight over landfill in historically Black Nashville neighborhood heads to court.

Wake County (2022), South Wake Landfill to Turn Landfill Gas into Renewable Natural Gas.

Zuo, X., W. Sun, I. D. Smedt, X. Li, S. Liu, D. Pu, S. Sun, J. Li, Y. Chen, W. Fu, P. Zhang, Y. Li, X. Yang, T.-M. Fu, H. Shen, J. Ye, C. Wang, and L. Zhu (2023), Observing downwind structures of urban HCHO plumes from space: Implications to non-methane volatile organic compound emissions, *preprint*, Preprints, doi:10.22541/essoar.169447462.22876028/v1.

Supplemental Figures

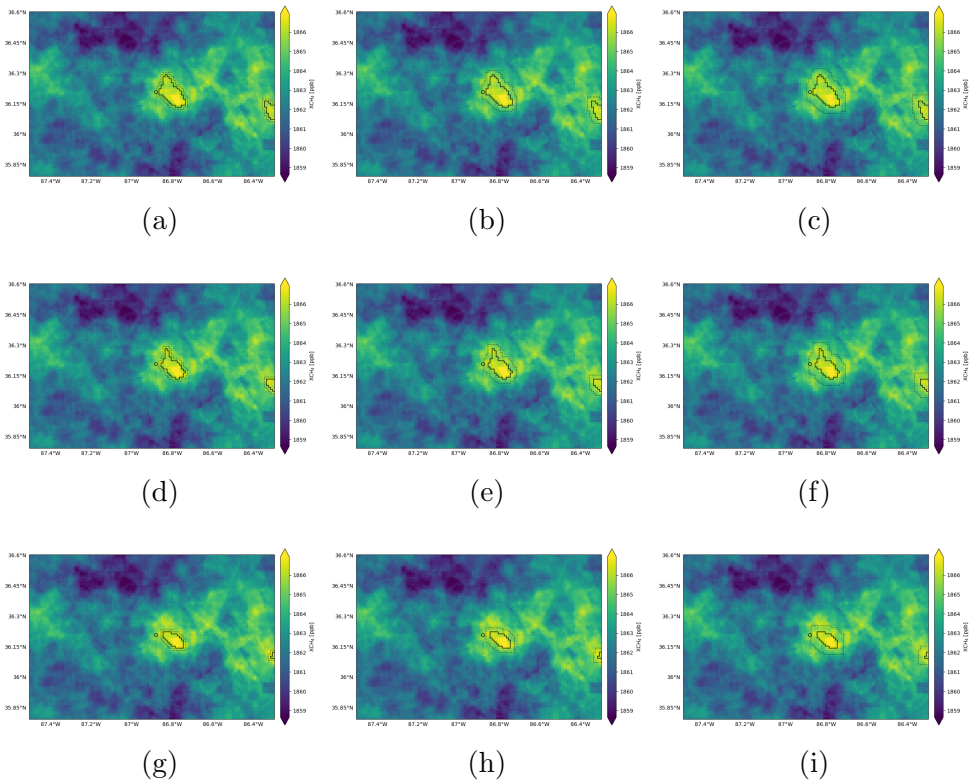

Figure 4.5: Oversampled region, wind-rotated around Bordeaux Landfill using 2019 data. Oversampled at 0.01°x 00.1°resolution. The solid black line delineates a plume. Bordeaux Landfill is marked with a black circle. The area between the dashed black line and the solid black line is considered the background. The plume is defined as the region above the (a-c) 98, (d-f) 98.5, or (g-i) 99 percentile. The background has a cell width beyond the plume perimeter of (a, d, g) 1 cell, (b, e, h) 2 cells, or (c, f, i) 3 cells.

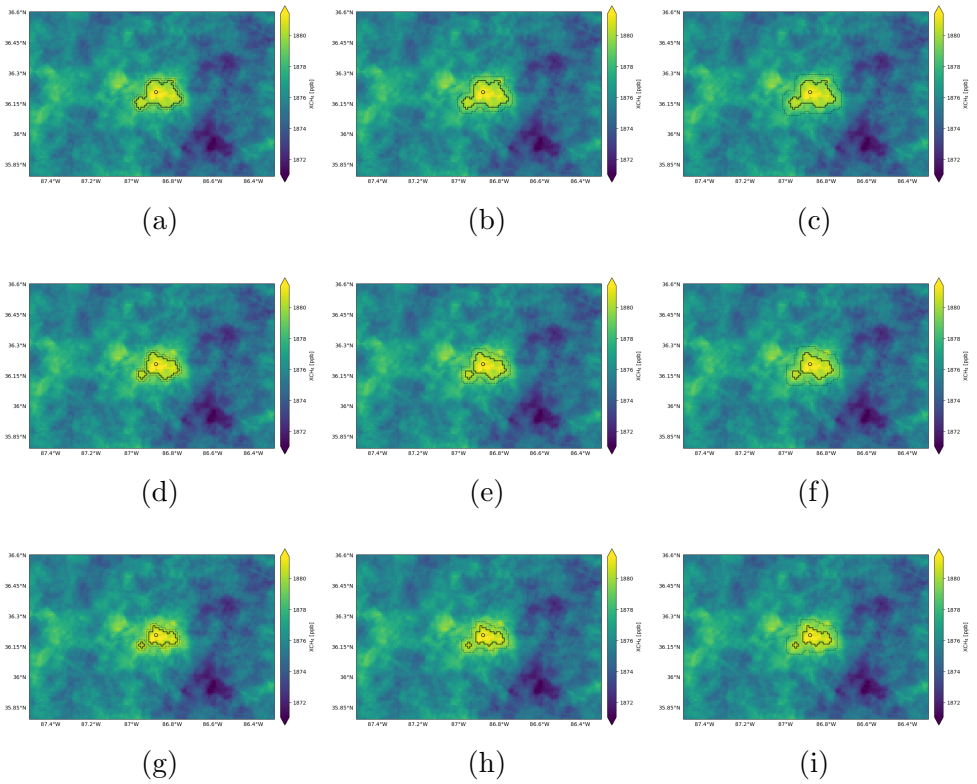

Figure 4.6: Oversampled region, wind-rotated around Bordeaux Landfill using 2020 data. Oversampled at 0.01°x 00.1°resolution. The solid black line delineates a plume. Bordeaux Landfill is marked with a black circle. The area between the dashed black line and the solid black line is considered the background. The plume is defined as the region above the (a-c) 98, (d-f) 98.5, or (g-i) 99 percentile. The background has a cell width beyond the plume perimeter of (a, d, g) 1 cell, (b, e, h) 2 cells, or (c, f, i) 3 cells.

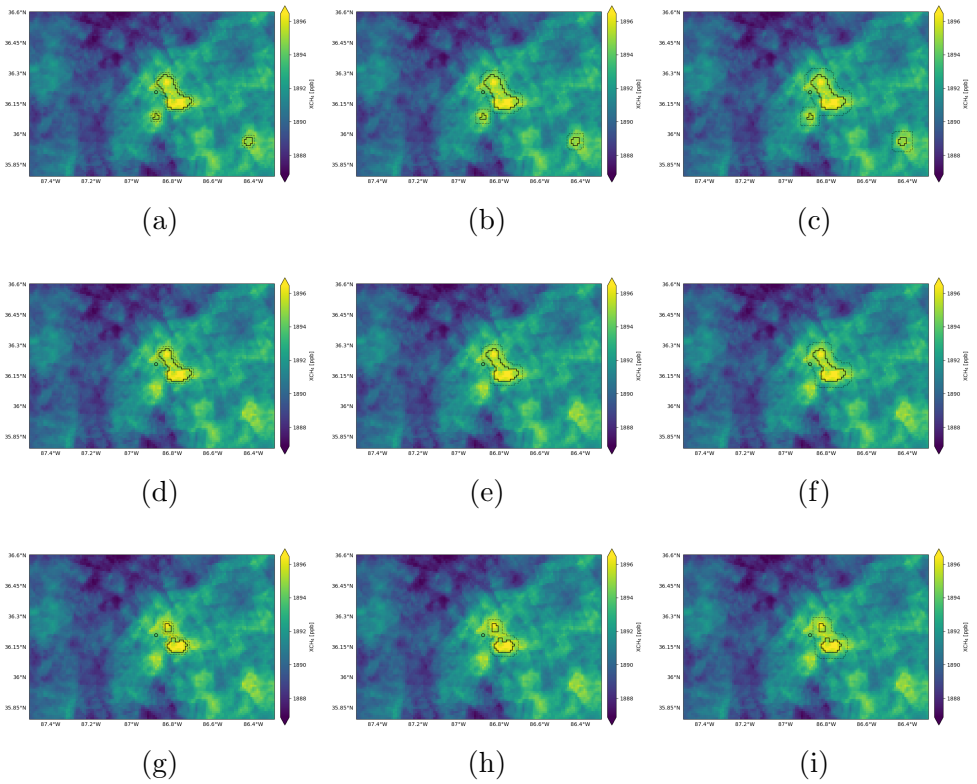

Figure 4.7: Oversampled region, wind-rotated around Bordeaux Landfill using 2021 data. Oversampled at 0.01°x 00.1°resolution. The solid black line delineates a plume. Bordeaux Landfill is marked with a black circle. The area between the dashed black line and the solid black line is considered the background. The plume is defined as the region above the (a-c) 98, (d-f) 98.5, or (g-i) 99 percentile. The background has a cell width beyond the plume perimeter of (a, d, g) 1 cell, (b, e, h) 2 cells, or (c, f, i) 3 cells.

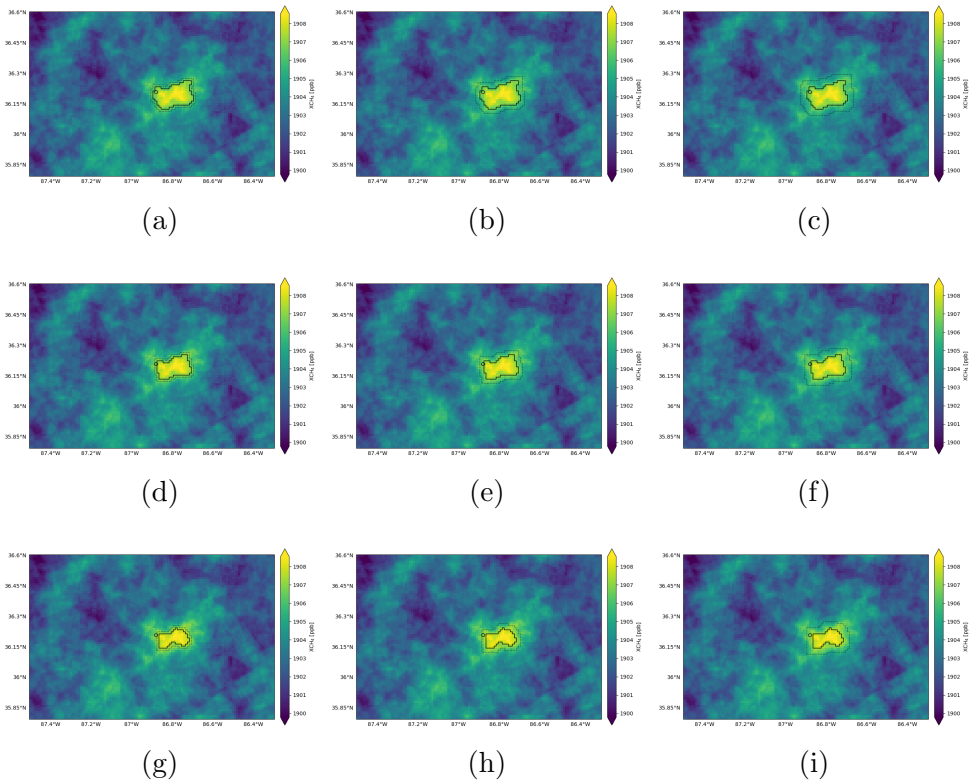

Figure 4.8: Oversampled region, wind-rotated around Bordeaux Landfill using 2022 data. Oversampled at 0.01°x 00.1°resolution. The solid black line delineates a plume. Bordeaux Landfill is marked with a black circle. The area between the dashed black line and the solid black line is considered the background. The plume is defined as the region above the (a-c) 98, (d-f) 98.5, or (g-i) 99 percentile. The background has a cell width beyond the plume perimeter of (a, d, g) 1 cell, (b, e, h) 2 cells, or (c, f, i) 3 cells.

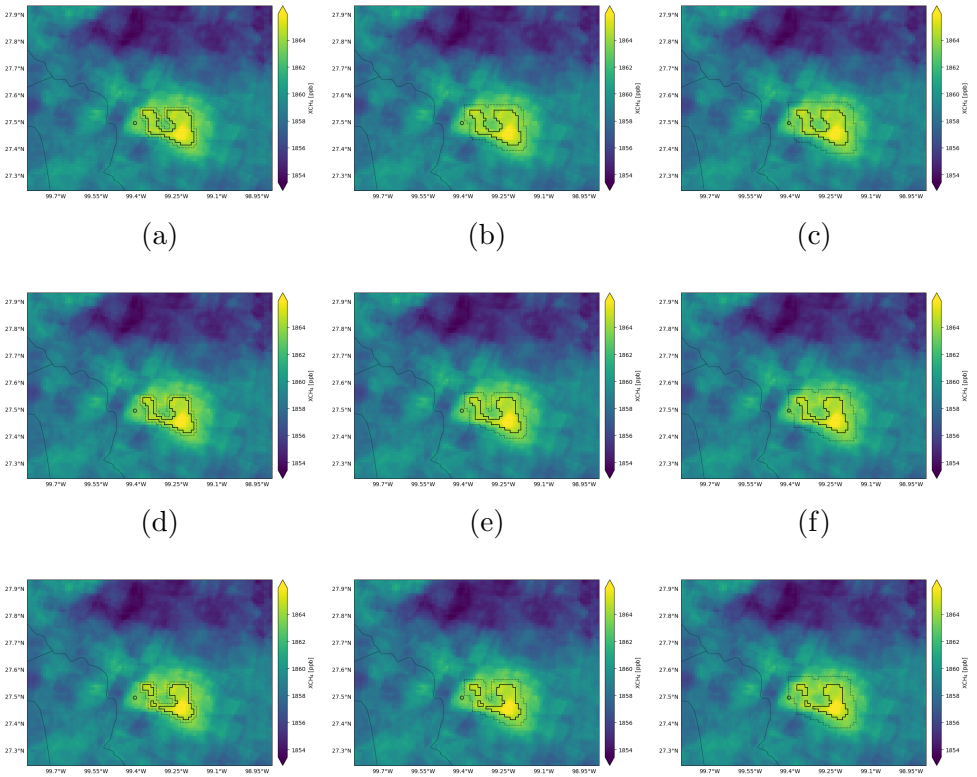

Figure 4.9: Oversampled region, wind-rotated around City of Laredo Landfill using 2019 data. Oversampled at 0.01°x 00.1°resolution. The solid black line delineates a plume. City of Laredo Landfill is marked with a black circle. The area between the dashed black line and the solid black line is considered the background. The plume is defined as the region above the (a-c) 97.75, (d-f) 98, or (g-i) 98.25 percentile. The background has a cell width beyond the plume perimeter of (a, d, g) 1 cell, (b, e, h) 2 cells, or (c, f, i) 3 cells.

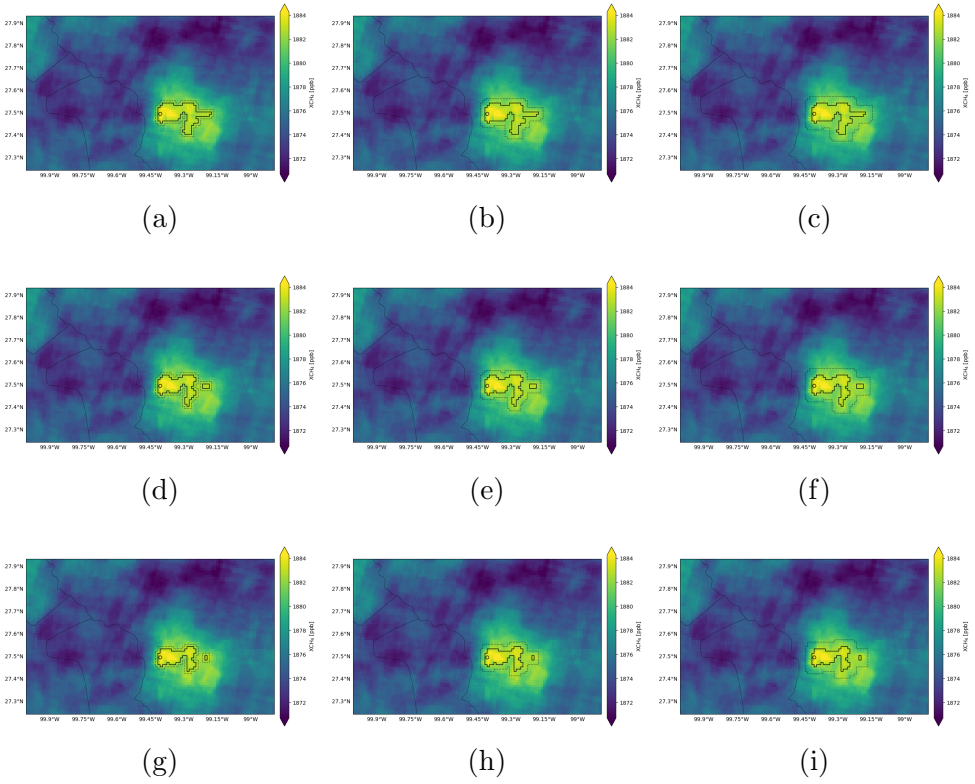

Figure 4.10: Oversampled region, wind-rotated around City of Laredo Landfill using 2020 data. Oversampled at 0.01°x 00.1°resolution. The solid black line delineates a plume. City of Laredo Landfill is marked with a black circle. The area between the dashed black line and the solid black line is considered the background. The plume is defined as the region above the (a-c) 98, (d-f) 98.25, or (g-i) 98.5 percentile. The background has a cell width beyond the plume perimeter of (a, d, g) 1 cell, (b, e, h) 2 cells, or (c, f, i) 3 cells.

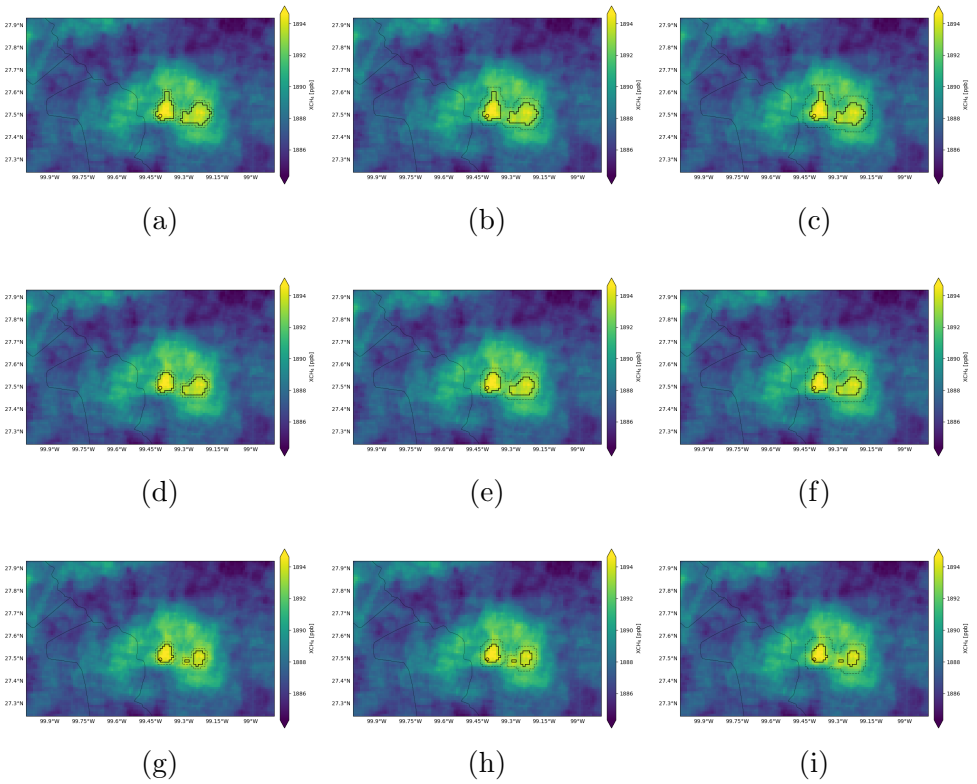

Figure 4.11: Oversampled region, wind-rotated around City of Laredo Landfill using 2021 data. Oversampled at 0.01°x 00.1°resolution. The solid black line delineates a plume. City of Laredo Landfill is marked with a black circle. The area between the dashed black line and the solid black line is considered the background. The plume is defined as the region above the (a-c) 98, (d-f) 98.5, or (g-i) 99 percentile. The background has a cell width beyond the plume perimeter of (a, d, g) 1 cell, (b, e, h) 2 cells, or (c, f, i) 3 cells.

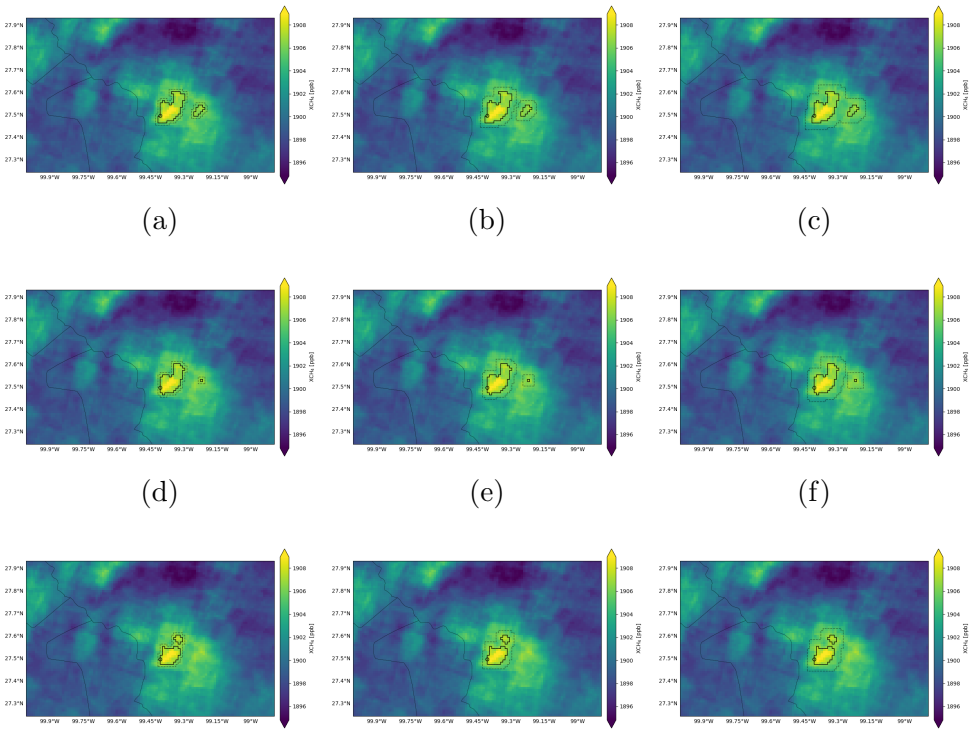

Figure 4.12: Oversampled region, wind-rotated around City of Laredo Landfill using 2022 data. Oversampled at 0.01°x 00.1°resolution. The solid black line delineates a plume. City of Laredo Landfill is marked with a black circle. The area between the dashed black line and the solid black line is considered the background. The plume is defined as the region above the (a-c) 98.5, (d-f) 98.75, or (g-i) 99 percentile. The background has a cell width beyond the plume perimeter of (a, d, g) 1 cell, (b, e, h) 2 cells, or (c, f, i) 3 cells.

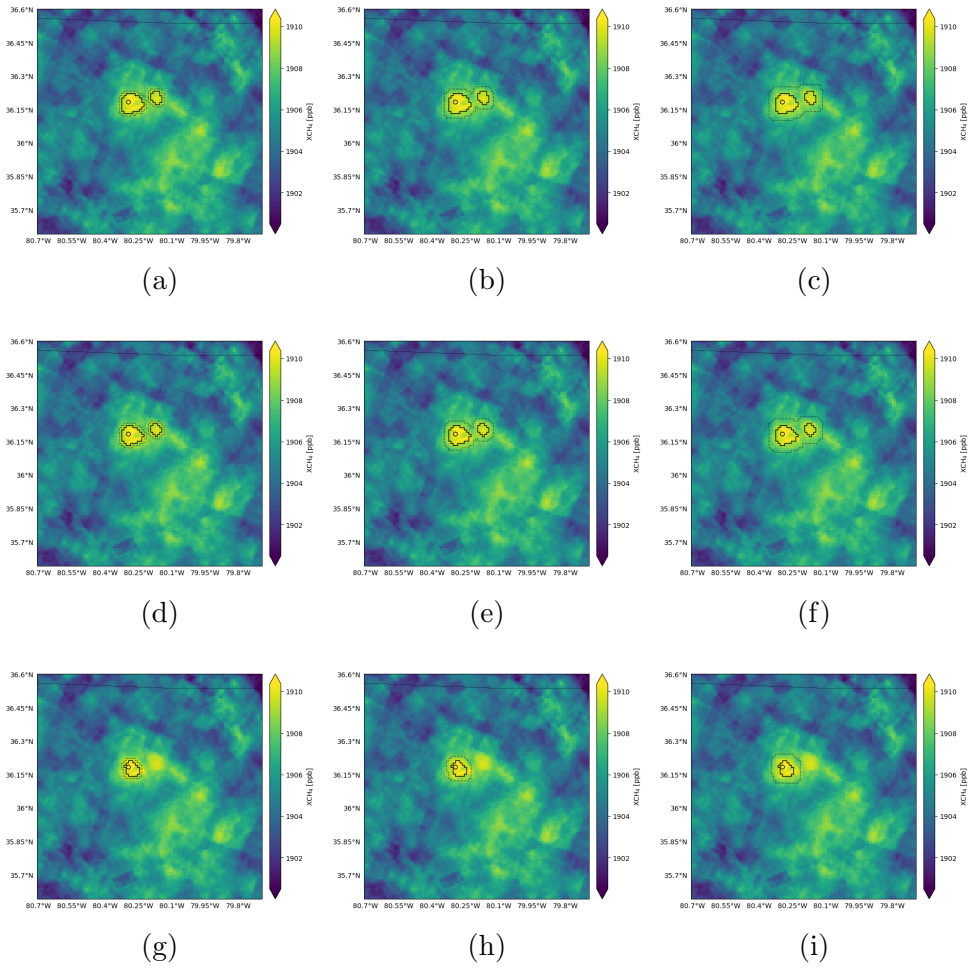

Figure 4.13: Oversampled region, wind-rotated around Hanes Mill Road Landfill using 2022 data. Oversampled at 0.01°x 00.1°resolution. The solid black line delineates a plume. Hanes Mill Road Landfill is marked with a black circle. The area between the dashed black line and the solid black line is considered the background. The plume is defined as the region above the (a-c) 98.75, (d-f) 99.00, or (g-i) 99.50 percentile. The background has a cell width beyond the plume perimeter of (a, d, g) 1 cell, (b, e, h) 2 cells, or (c, f, i) 3 cells.

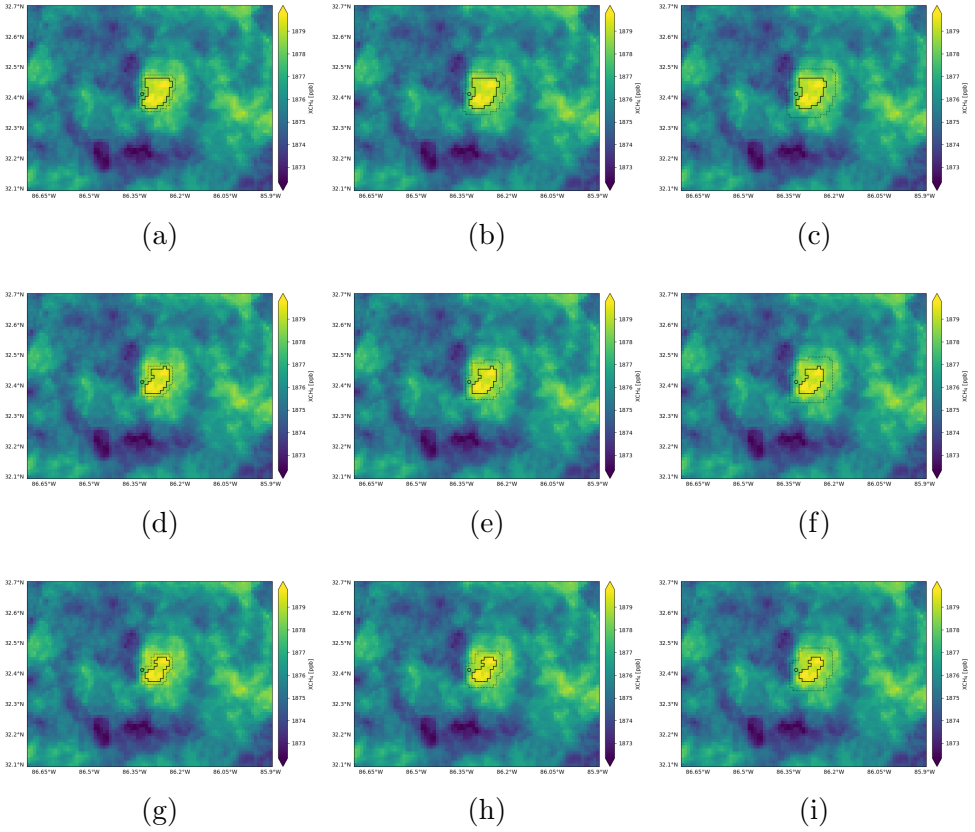

Figure 4.14: Oversampled region, wind-rotated around Montgomery City of Landfill using 2020 data. Oversampled at 0.01°x 00.1°resolution. The solid black line delineates a plume. Montgomery City of Landfill is marked with a black circle. The area between the dashed black line and the solid black line is considered the background. The plume is defined as the region above the (a-c) 98.50, (d-f) 99.00, or (g-i) 99.25 percentile. The background has a cell width beyond the plume perimeter of (a, d, g) 1 cell, (b, e, h) 2 cells, or (c, f, i) 3 cells.

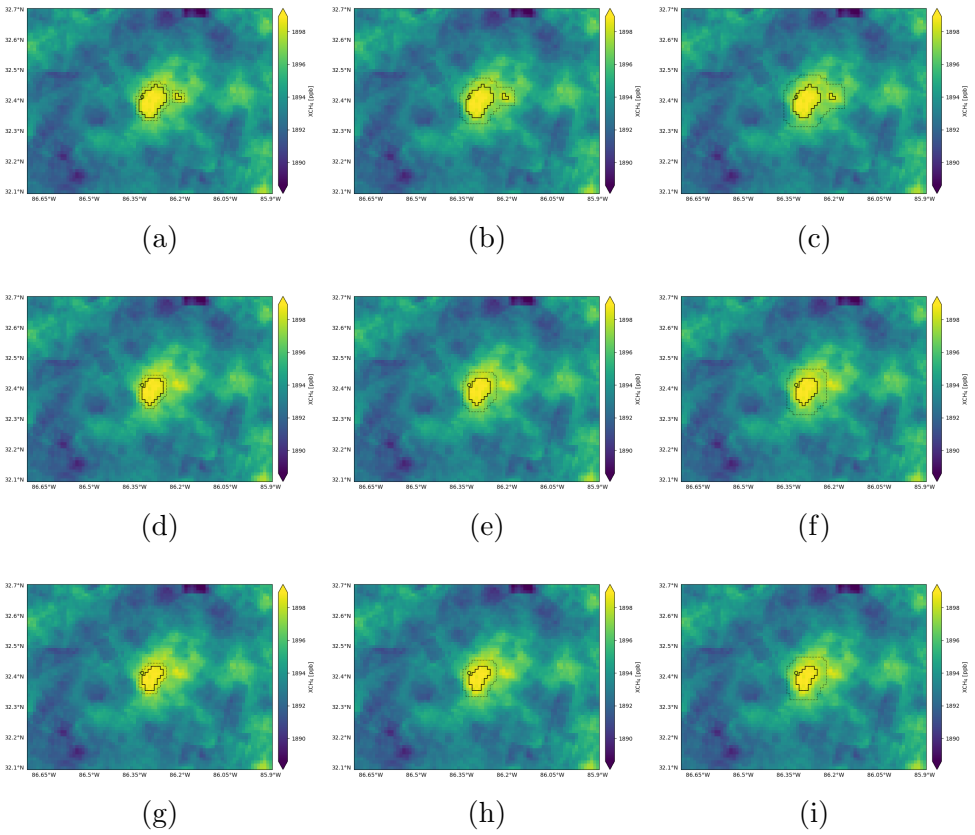

Figure 4.15: Oversampled region, wind-rotated around Montgomery City of Landfill using 2021 data. Oversampled at 0.01°x 00.1°resolution. The solid black line delineates a plume. Montgomery City of Landfill is marked with a black circle. The area between the dashed black line and the solid black line is considered the background. The plume is defined as the region above the (a-c) 98.50, (d-f) 99.00, or (g-i) 99.25 percentile. The background has a cell width beyond the plume perimeter of (a, d, g) 1 cell, (b, e, h) 2 cells, or (c, f, i) 3 cells.

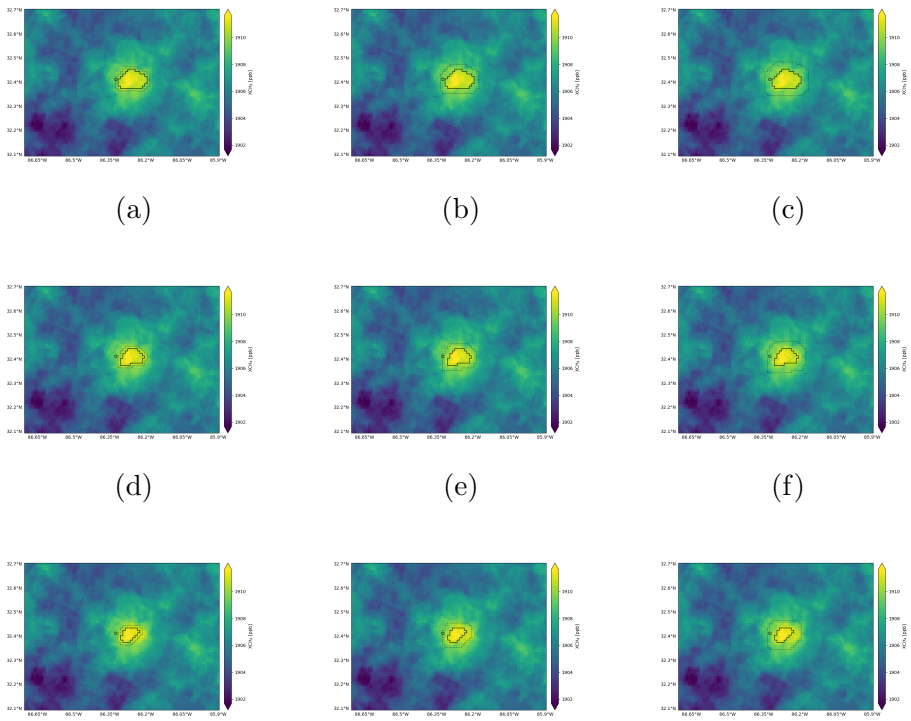

(a) (b) (c)

(d) (e) (f)

(g) (h) (i)

Figure 4.16: Oversampled region, wind-rotated around Montgomery City of Landfill using 2022 data. Oversampled at 0.01°x 00.1°resolution. The solid black line delineates a plume. Montgomery City of Landfill is marked with a black circle. The area between the dashed black line and the solid black line is considered the background. The plume is defined as the region above the (a-c) 98.50, (d-f) 99.00, or (g-i) 99.25 percentile. The background has a cell width beyond the plume perimeter of (a, d, g) 1 cell, (b, e, h) 2 cells, or (c, f, i) 3 cells.

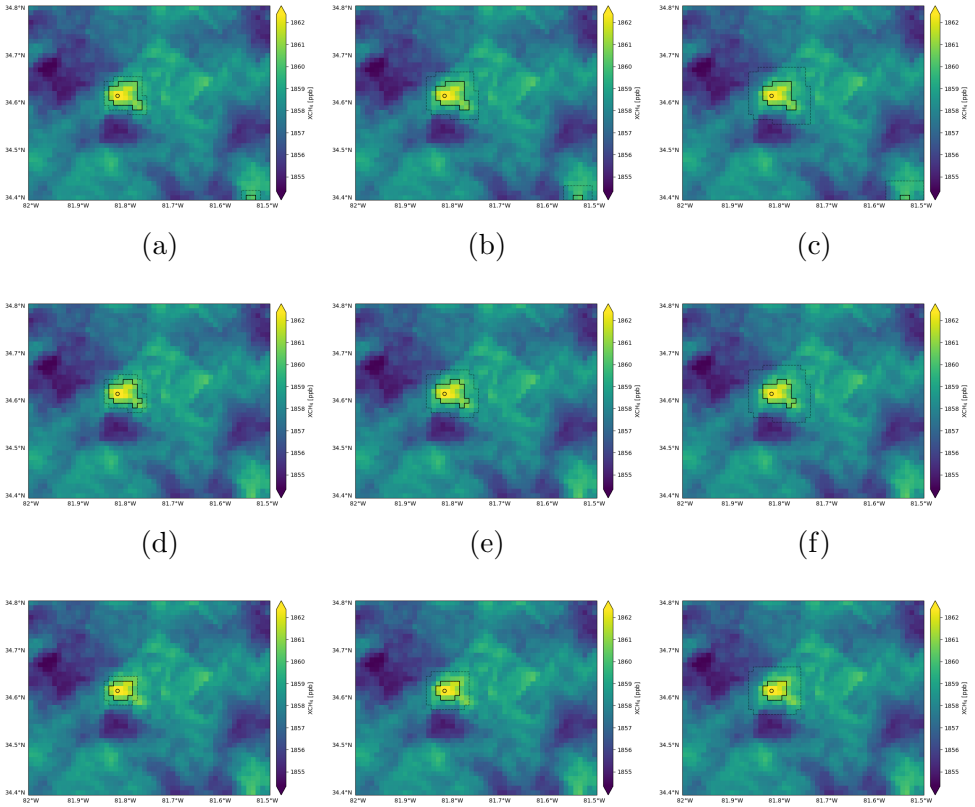

Figure 4.17: Oversampled region, wind-rotated around Union County Landfill using 2019 data. Oversampled at 0.01°x 00.1°resolution. The solid black line delineates a plume. Union County Landfill is marked with a black circle. The area between the dashed black line and the solid black line is considered the background. The plume is defined as the region above the (a-c) 98.00, (d-f) 98.50, or (g-i) 99.00 percentile. The background has a cell width beyond the plume perimeter of (a, d, g) 1 cell, (b, e, h) 2 cells, or (c, f, i) 3 cells.

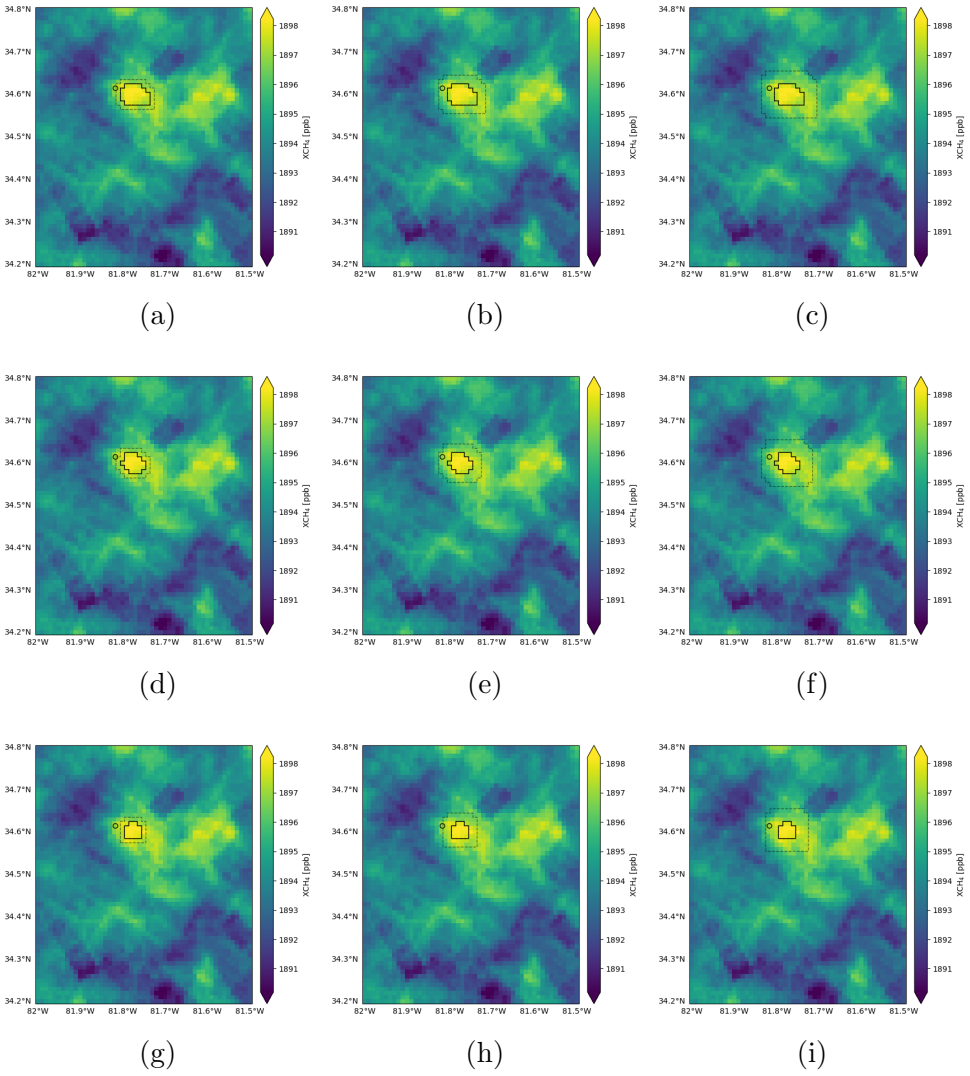

Figure 4.18: Oversampled region, wind-rotated around Union County Landfill using 2021 data. Oversampled at 0.01°x 00.1°resolution. The solid black line delineates a plume. Union County Landfill is marked with a black circle. The area between the dashed black line and the solid black line is considered the background. The plume is defined as the region above the (a-c) 98.00, (d-f) 98.50, or (g-i) 99.00 percentile. The background has a cell width beyond the plume perimeter of (a, d, g) 1 cell, (b, e, h) 2 cells, or (c, f, i) 3 cells.

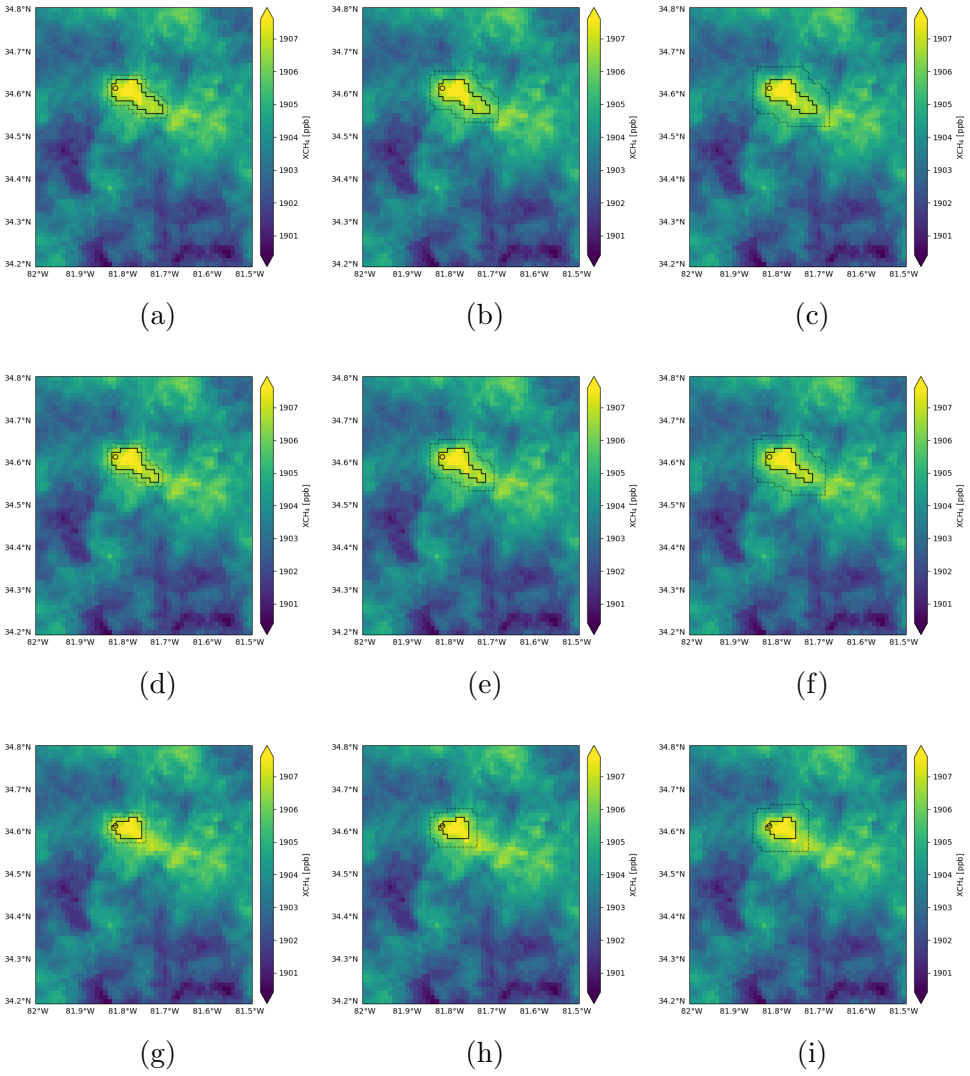

Figure 4.19: Oversampled region, wind-rotated around Union County Landfill using 2022 data. Oversampled at 0.01°x 00.1°resolution. The solid black line delineates a plume. Union County Landfill is marked with a black circle. The area between the dashed black line and the solid black line is considered the background. The plume is defined as the region above the (a-c) 98.00, (d-f) 98.50, or (g-i) 99.00 percentile. The background has a cell width beyond the plume perimeter of (a, d, g) 1 cell, (b, e, h) 2 cells, or (c, f, i) 3 cells.

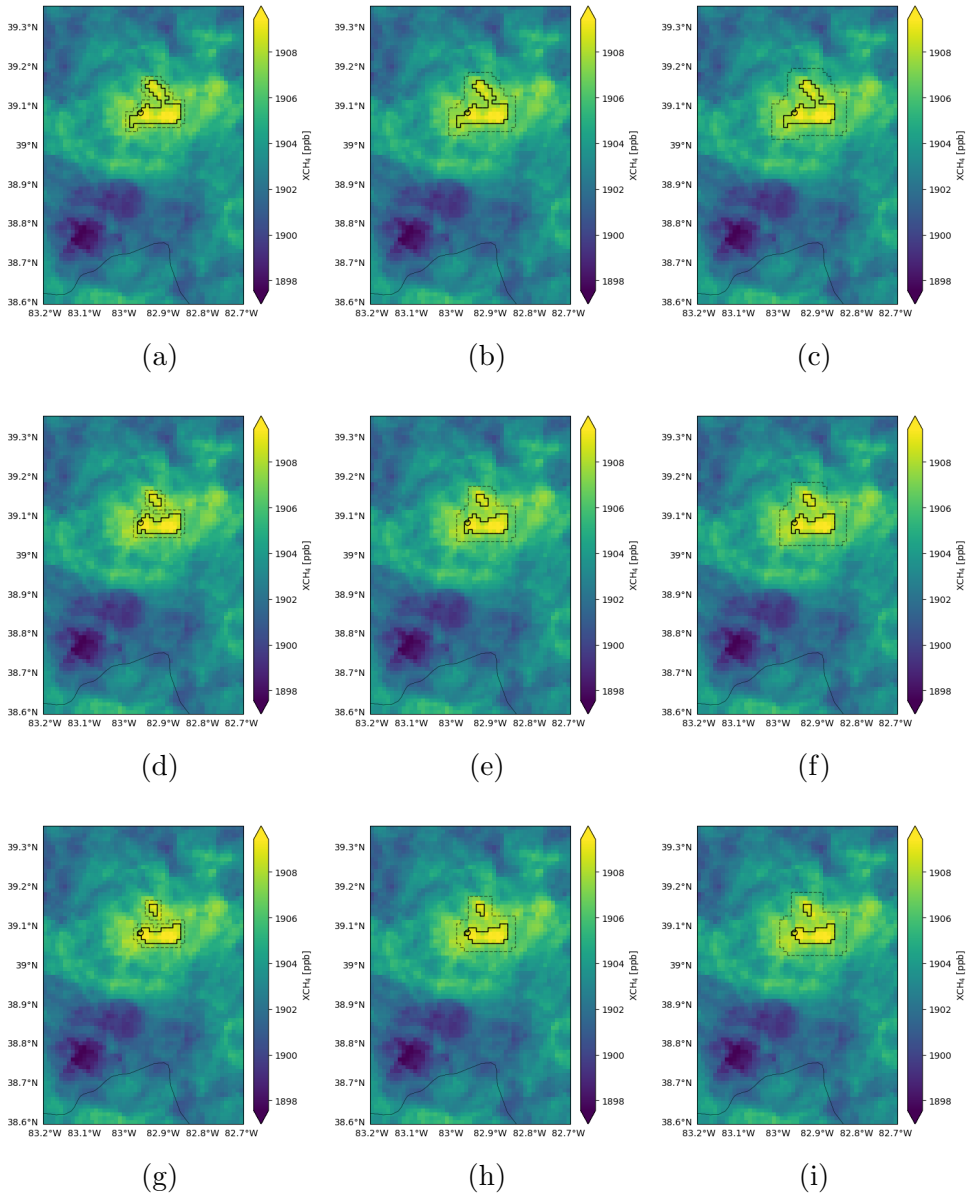

Figure 4.20: Oversampled region, wind-rotated around Pike Sanitation Inc. using 2022 data. Oversampled at 0.01°x 00.1°resolution. The solid black line delineates a plume. Pike Sanitation Inc. is marked with a black circle. The area between the dashed black line and the solid black line is considered the background. The plume is defined as the region above the (a-c) 98.00, (d-f) 98.50, or (g-i) 98.75 percentile. The background has a cell width beyond the plume perimeter of (a, d, g) 1 cell, (b, e, h) 2 cells, or (c, f, i) 3 cells.

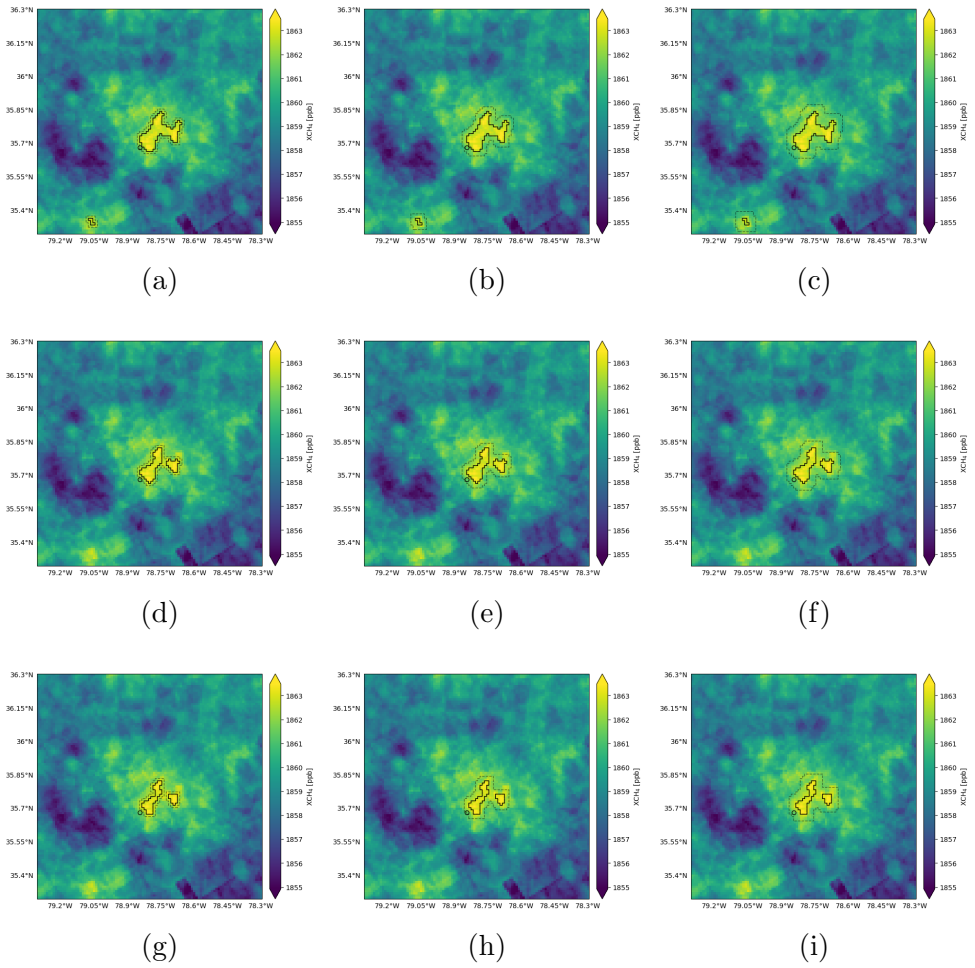

Figure 4.21: Oversampled region, wind-rotated around South Wake Landfill using 2019 data. Oversampled at 0.01°x 00.1°resolution. The solid black line delineates a plume. South Wake Landfill is marked with a black circle. The area between the dashed black line and the solid black line is considered the background. The plume is defined as the region above the (a-c) 98.50, (d-f) 99.00, or (g-i) 99.25 percentile. The background has a cell width beyond the plume perimeter of (a, d, g) 1 cell, (b, e, h) 2 cells, or (c, f, i) 3 cells.

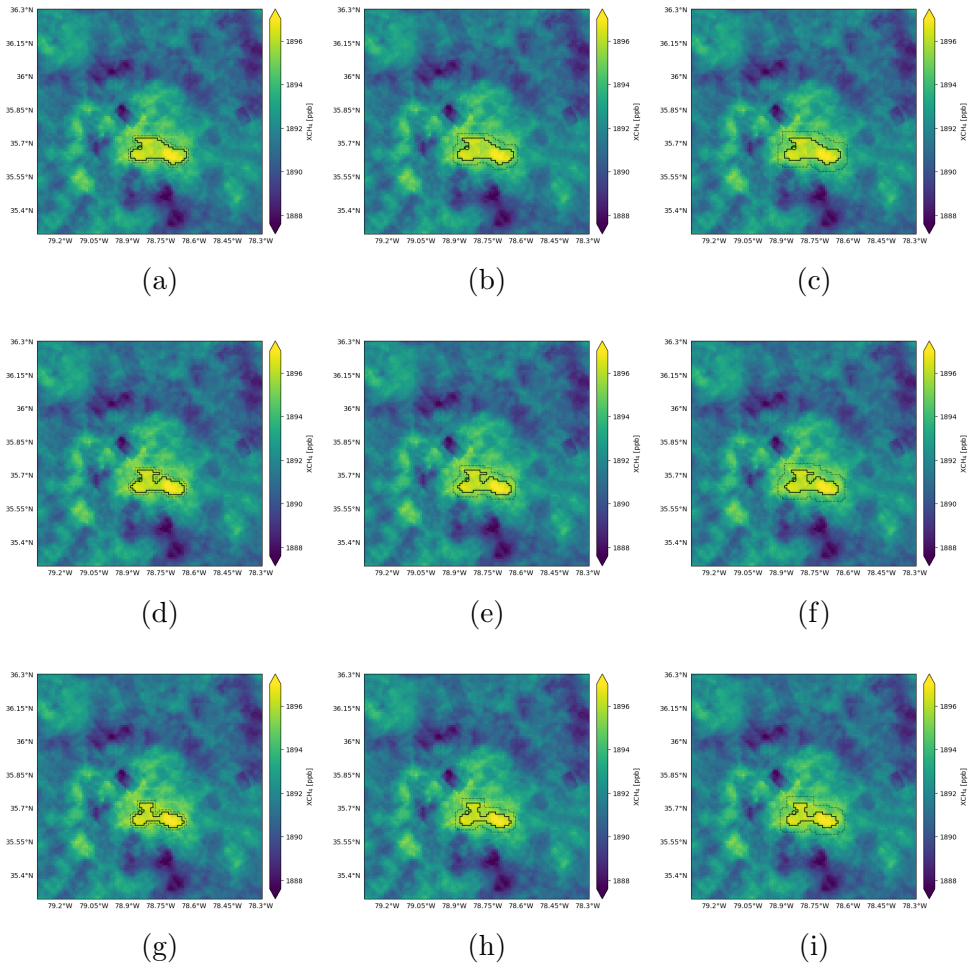

Figure 4.22: Oversampled region, wind-rotated around South Wake Landfill using 2021 data. Oversampled at 0.01°x 00.1°resolution. The solid black line delineates a plume. South Wake Landfill is marked with a black circle. The area between the dashed black line and the solid black line is considered the background. The plume is defined as the region above the (a-c) 98.25, (d-f) 98.50, or (g-i) 98.75 percentile. The background has a cell width beyond the plume perimeter of (a, d, g) 1 cell, (b, e, h) 2 cells, or (c, f, i) 3 cells.

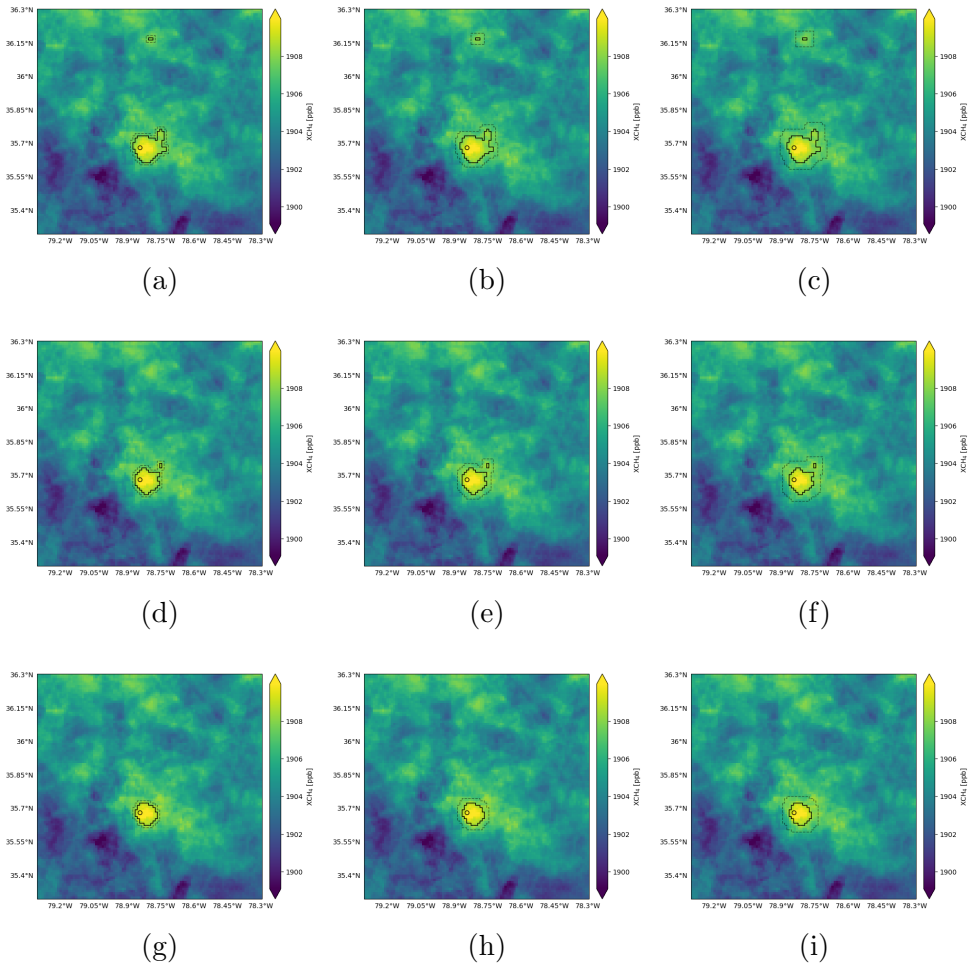

Figure 4.23: Oversampled region, wind-rotated around South Wake Landfill using 2022 data. Oversampled at 0.01°x 00.1°resolution. The solid black line delineates a plume. South Wake Landfill is marked with a black circle. The area between the dashed black line and the solid black line is considered the background. The plume is defined as the region above the (a-c) 98.50, (d-f) 99.00, or (g-i) 99.25 percentile. The background has a cell width beyond the plume perimeter of (a, d, g) 1 cell, (b, e, h) 2 cells, or (c, f, i) 3 cells.